AD-A111 123 AIR FORCE INST OF TECH WRIGHT-PATTERSON AFB OH SCHOO--ETC F/G 20/4
FINITE ELEMENT ANALYSIS OF SUBSONIC FLOW OVER A LIFTING THIN AI--ETC(U)
DEC 81 J C GAY
UNCLASSIFIED AFIT/GAE/AA/81D-11 NL

1 OF 1
AD A
111123

END
DATE
FILMED
03-82
DTIC

(1) LEVEL II

AD A111123

DTIC FILE COPY

DTIC
ELECTE
FEB 19 1982
S D
B

UNITED STATES AIR FORCE

AIR UNIVERSITY

AIR FORCE INSTITUTE OF TECHNOLOGY

Wright-Patterson Air Force Base, Ohio

DISTRIBUTION STATEMENT A
Approved for public release;
Distribution Unlimited

82 02 18 073

(1) LEVEL

AFIT/GAE/AA/81D-11

FINITE ELEMENT ANALYSIS OF

SUBSONIC FLOW OVER

A LIFTING THIN AIRFOIL

THESIS

AFIT/GAE/AA/81D-11 John C. Gay
Capt USAF

Approved for public release; distribution unlimited

DTIC
ELECTE
FEB 10 1982
S D
B

AFIT/GAE/AA/81D-11

FINITE ELEMENT ANALYSIS OF SUBSONIC FLOW OVER A LIFTING THIN AIRFOIL

THESIS

Presented to the Faculty of the School of Engineering

of the Air Force Institute of Technology

Air University

in Partial Fulfillment of the

Requirements for the Degree of

Master of Science

by

John C. Gay, B.S.

Capt USAF

Graduate Aeronautical Engineering

December 1981

Approved for public release; distribution unlimited

Preface

During my first three quarters at the Air Force Institute, I was fortunate enough to take courses in both Aerodynamics and Structural Mechanics, two areas of interest to me as an undergraduate. When this thesis subject was presented as a possible thesis topic, I saw the opportunity to apply knowledge learned in the two areas of interest and thus chose this topic.

My thanks go to my advisor, Capt James Marsh, whose classroom instruction and advice laid the groundwork necessary for me to complete the work done here.

My greatest thanks go to my wife, Claire, who had to put up with me during the time spent working on this thesis.

John C. Gay

Distribution/
Availability Codes
Avail and/or
Dist Special
A

Contents

Preface ii

List of Figures iv

Abstract vi

I. Introduction 1

History and Previous Work 1
Objective 3

II. Thin Airfoil Problem Formulation 5

Method of Small Perturbations 7
The Finite Element Approximation 10
Treatment of Farfield Boundary 13

III. Solution Methods 15

Superposition 15
Iterative Method 1 17
Iterative Method 2 17

IV. The Flat-Plate at Angle of Attack 19

Flowfield Grid Parameters 19
Linear Elements 20
Farfield Boundary Location 20
Pressure Coefficient 24
Mixed Elements 32
Farfield Boundary Location 40
Pressure Coefficient 40
Quadratic Elements 45
Farfield Boundary Location 45
Pressure Coefficient 47

V. Conclusions and Recommendations 55

Bibliography 59

Appendix A: Finite Element Equations For Flow Over an Airfoil For a Bilinear, Rectangular Element ... 61

Appendix B: Finite Element Equations For Flow Over an Airfoil For a Biquadratic, Lagrange, Rectangular Element 67

Appendix C: Finite Element Equations For Flow Over an Airfoil For a Mixed, Rectangular Element 73

Vita 77

List of Figures

Figure		Page
1	Flowfield	6
2	Airfoil Problem Superposition	11
3	Linear Equally Spaced Element Discretization	21
4	Linear Equally Spaced Element Discretization With Small Trailing Edge Element	22
5	Linear Exponentially Spaced Element Discretization	23
6	Linear Elements, Constant Aspect Ratio, Expansion of Domain in x-direction	25
7	Linear Elements, Constant Aspect Ratio, Expansion of Domain in y-direction	26
8	Convergence of Circulation For Linear Element Grids	27
9	Pressure Distribution For Linear Equally Spaced Elements and Uniform Reduction of Element Size	29
10	Pressure Distribution For Linear Equally Spaced Elements With Small Trailing Edge Element and Uniform Reduction of Element Size	30
11	Pressure Distribution For Linear Exponentially Spaced Elements and Uniform Reduction of Element Size	31
12	Pressure Distribution For Linear Equally Spaced Elements and Uniform Reduction of Farfield Parameters Only	33
13	Pressure Distribution For Linear Equally Spaced Elements With Small Trailing Edge Element and Uniform Reduction of Farfield Parameters Only	34
14	Pressure Distribution For Linear Exponentially Spaced Elements and Uniform Reduction of Farfield Parameters Only	35
15	Pressure Distribution For Linear Equally Spaced Elements and Uniform Reduction of Airfoil Element Width Parameter	36
16	Pressure Distribution For Linear Equally Spaced Elements With Small Trailing Edge Element and Uniform Reduction of Airfoil Element Width Parameter	37

Figure		Page

17 Pressure Distribution For Linear Exponentially Spaced Elements and Uniform Reduction of Airfoil Width Parameter 38

18 Mixed Element Discretization 39

19 Mixed Elements, Constant Aspect Ratio, Expansion of Domain in x-direction 41

20 Mixed Elements, Constant Aspect Ratio, Expansion of Domain in y-direction 42

21 Convergence of Circulation of Mixed Elements Compared to Linear Equally Spaced Grids 43

22 Pressure Distribution For Mixed Elements and Uniform Reduction of Element Size 44

23 Quadratic Element Discretization 46

24 Quadratic Elements, Constant Aspect Ratio, Expansion of Domain in x-direction 48

25 Quadratic Elements, Constant Aspect Ratio, Expansion of Domain in y-direction 49

26 Pressure Distribution for Quadratic Elements and Uniform Reduction of Element Size 50

27 Pressure Distribution for Quadratic Elements and Uniform Reduction of Farfield Parameters Only 51

28 Pressure Distribution for Quadratic Elements and Reduction of Airfoil Element Width Parameter Only 53

29 Pressure Distribution Comparison of Linear, Mixed, and Quadratic Elements 54

30 Bilinear Rectangular Element 62

31 Biquadratic, Lagrange, Element 68

32 Element Stiffness Matrix for the Quadratic, Lagrange, Element 70

33 Mixed Rectangular Element 74

Abstract

The finite element method was used to solve the flow field problem around a thin, lifting, flat plate, airfoil. The governing equation solved is the Laplace equation, which is valid for inviscid, irrotational, incompressible flow.

The finite element equations were derived through the method of weighted residuals with weighting functions selected by the Galerkin method. For the purposes of analysis, the infinite flow field was replaced by a finite domain. Neumann type boundary conditions were imposed on the airfoil surface. Dirichlet boundary conditions were specified as required by the problem formulation for uniqueness.

Three types of solution methods were used, for various treatments of the jump discontinuity required in the lifting problem. The first method was a superposition technique, which treated the potential along the upper and lower nodes of the branch cut as constant. The circulation was determined by applying the Kutta condition during the combination of the subproblems. The second method was an iterative technique where the circulation was varied until the Kutta condition was satisfied. This method also specified constant potential along the upper and lower branch cut nodes. The third method was also an iterative technique on circulation; however, only the ratio of potentials across the branch cut nodes were kept constant.

Three types of elements were investigated to approximate the solution for the velocity potential function. The first was a bilinear rectangular

element. The second was a mixed element with three linear sides and one quadratic side used only on the airfoil surface. All other elements used with it were bilinear. The third element used was a biquadratic, Lagrange, element. The convergence characteristics of each element were studied as a function of the discretization. The pressure distributions are compared with those of classical thin-airfoil theory.

FINITE ELEMENT ANALYSIS OF SUBSONIC FLOW OVER A LIFTING THIN AIRFOIL

I Introduction

In the design of aircraft lifting surfaces, it is important to select a design that has a high probability of meeting desired characteristics. Because of the large costs associated with the construction and test of models, computational techniques for predicting the performance of these designs have evolved with aircraft technology. Over the past 25 years, the most extensively used method in the aircraft industry has been the finite difference method. This method; however, becomes difficult to apply when complex geometries, multiply connected domains, or complex boundary conditions are involved. Finite element methods can overcome some of these difficulties, through easier treatment of complex geometries and a more consistant method of using higher-order approximations (Ref 1). For these reasons the finite element has been increasingly utilized in solution of fluids problems. The treatment of the flowfield as a two-dimensional potential flow problem, although the flow is in fact more complex, is a reasonable simplification since the selection of a suitable section shape is an important part of the design process. The application of this method to the thin lifting airfoil is a good first step in the solution of the general airfoil problem. A further simplification can be made by assuming incompressible flow, thus reducing the problem to solution of the Laplace equation.

History and Previous Work

The finite element method was developed by aircraft structural

engineers in the 1950's, to analyze large structural problems in aircraft. These early developments were the result of applying matrix methods, which were successful with discrete structures, to continuous ones. The first description of the procedure was presented in 1956 by a group (Turner, Clough, Martin, and Topp) at the Boeing Aircraft Company. The extension of the finite element method to non-structural problems began in the early 1960's. Finite element analysis is closely related to the classical variational concepts of the Rayleigh-Ritz method or the weighted residual methods modeled after the method of Galerkin, thus it has been established as an important branch of approximation theory (Ref 2 and 3).

The first paper to propose the extension of the finite element method to continuum problems involving the Laplace equation was by Zienkiewiez and Cheung in 1965 (Ref 4). In 1968, Martin (Ref 5) using linear triangular elements and a variational principle formulation solved for the stream function for incompressible flow over a circular cylinder between two parallel walls. Norrie and de Vries (Ref 6-8) in 1969 developed finite element techniques for solving incompressible flow problems over single and multiple airfoils. They used a variational principle to produce the finite element equations and formulated the problem in terms of both velocity potential and stream functions with linear triangular elements. The velocity potential solution involved the linear superposition of a thickness problem and a lifting problem. The combination of the two problems and application of the Kutta condition at the sharp trailing edge resulted in the specification of the circulation. This approach was also used by Carey (Ref 9) who extended it to compressible flow..

Shen (Ref 10) formulated the problem of incompressible flow over a lifting airfoil in terms of the stream function using a variational principle to develop the finite element equations. In this case, Shen treated the infinite domain as an inner and outer patch. The inner patch contained the airfoil and a portion of the flowfield at an arbitrary but sufficiently distant boundary. Only this inner patch was solved through finite element procedures, with linear triangular elements. In the outer patch an analytic solution with unknown coefficients was used. The two solutions were matched at the common boundary. The arbitrary airfoil was transformed through a Joukowski transformation to a near circle. This procedure was also used by Habashi (Ref 11) who used a Laurent series for the solution in the outer patch. He notes that this technique produces the value of circulation without integrating the pressure distribution, and serves to magnify regions of high gradients, at the leading and trailing edges. Recently, Baskharone and Hamed (Ref 12) developed a technique for treating the circulation around the airfoil as an additional variable, the value of which is directly calculated in the solution process, rather than an externally imposed condition. This is done by treating the circulation as a nodeless variable. A potential function formulation was used with linear triangular elements and parabolic quadrilateral isoparametric elements. Results are given for both a single airfoil and a cascade airfoil.

Objective

The purpose of this work was to compare the ability of several different finite element formulations to predict the surface pressure distributions for two-dimensional potential flow over a thin airfoil in an infinite uniform flowfield for incompressible subsonic flow. The

results were compared with known exact solutions. The assumptions traditionally used in classical thin-airfoil and small disturbance theories were used wherever necessary to simplify the problem. Three types of rectangular finite elements were used: linear; mixed, a transition element with three linear sides and one quadratic side aligned along the airfoil surface; and quadratic, lagrange, elements.

II Thin Airfoil Problem Formulation

The problem being considered is one of steady, two-dimensional, incompressible, inviscid, irrotational flow about a thin airfoil in a uniform stream of infinite domain. Let the freestream be taken to be directed in the positive x-direction, with the coordinate system attached at the midpoint of the airfoil. The symbol Ω denotes the infinite flowfield domain, with points (x,y), as shown in Fig 1. The boundary of Ω (denoted $\partial\Omega$) is composed of all points on the airfoil surface and the boundary at infinity. Because of circulation, a branch cut is placed in Ω.

For an irrotational flowfield, a velocity potential exists, such that the governing differential equation for incompressible flow is the Laplace equation

$$\nabla^2 \Phi(x,y) = 0 \qquad \text{for } (x,y) \text{ in } \Omega \qquad (1)$$

where Φ is the velocity potential function. The boundary conditions are

$$\nabla \Phi \cdot \nabla F = 0 \qquad ; \quad F(x,y) = 0 \qquad (2)$$

where $F(x,y)=0$ describes the airfoil profile, and the infinity condition

$$\nabla \Phi \rightarrow (U_\infty, 0) \qquad \text{as } (x,y) \rightarrow \infty \qquad (3)$$

where U_∞ is the free-stream velocity. For the lifting case, the Kutta condition must be satisfied, which requires the circulation (Γ) be

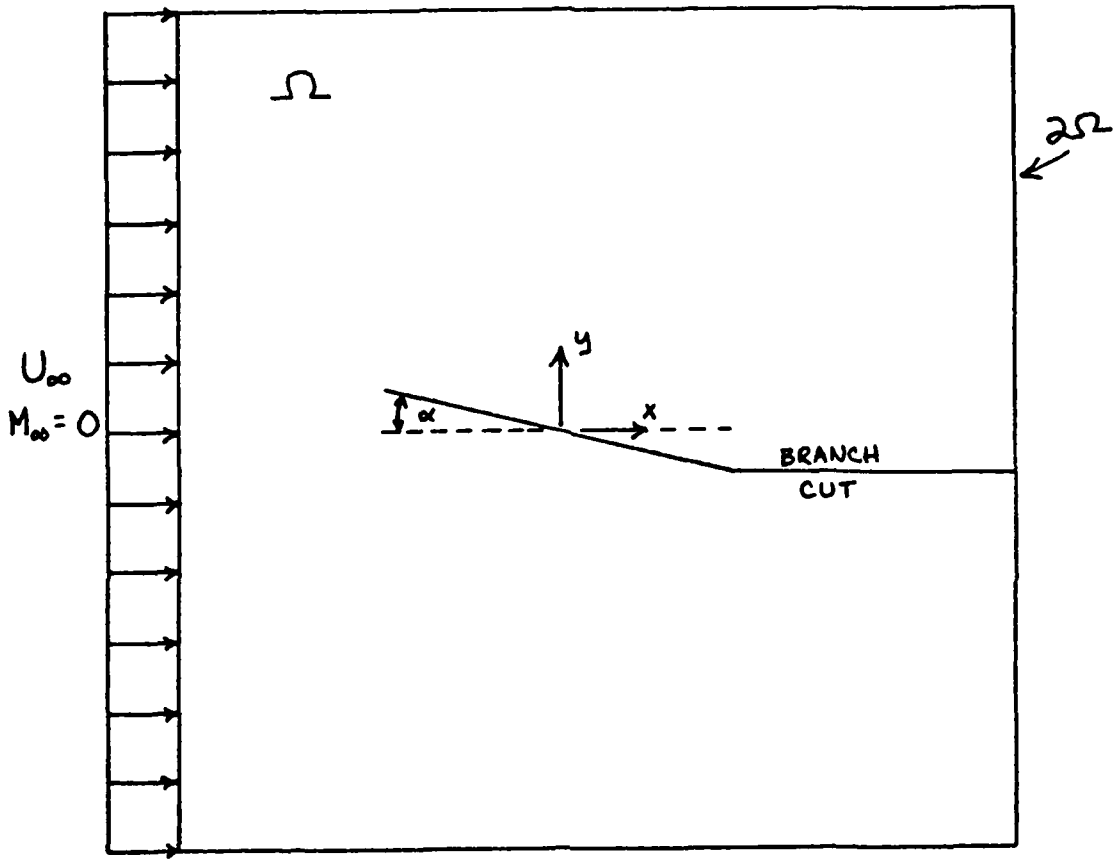

Figure 1. Flowfield

such that the velocity is finite at the trailing edge.

Method of Small Perturbations

The total velocity potential Φ can be expressed as the sum of the velocity potential due to the free stream and a perturbation potential ϕ (Ref 13),

$$\Phi = U_\infty(x + \phi) \tag{4}$$

where U_∞ is the free stream velocity and ϕ is the perturbation potential. The perturbation potential has velocity components u and v in the x- and y- direction respectively defined by

$$u = \frac{\partial \phi}{\partial x} \qquad v = \frac{\partial \phi}{\partial y} \tag{5}$$

Taking partial derivatives

$$\begin{aligned} \Phi_x &= U_\infty(1 + \phi_x) & \Phi_y &= U_\infty \phi_y \\ \Phi_{xx} &= U_\infty \phi_{xx} & \Phi_{yy} &= U_\infty \phi_{yy} \end{aligned} \tag{6}$$

Since $\nabla^2 \Phi = \Phi_{xx} + \Phi_{yy} = 0$ then also

$$\nabla^2 \phi = 0 \qquad \text{for } (x,y) \text{ in } \Omega \tag{7}$$

The boundary condition on the airfoil surface is now

$$(\bar{U}_\infty + \nabla\phi) \cdot \nabla F = 0 \quad ; \quad F(x,y) = 0 \tag{8}$$

The dot product is then

$$\left(\bar{U}_\infty + \frac{\partial \phi}{\partial x} \right) \frac{\partial F}{\partial x} + \frac{\partial \phi}{\partial y} \frac{\partial F}{\partial y} = 0 \tag{9}$$

The airfoil surface is described by

$$y = \eta(x) \tag{10}$$

then

$$F(x,y) = \eta(x) - y = 0 \tag{11}$$

and

$$\frac{\partial F}{\partial x} = \frac{d\eta}{dx} \qquad \frac{\partial F}{\partial y} = -1 \tag{12}$$

Substituting (12) into (9) results in

$$\frac{\partial \phi}{\partial y} = \left(U_\infty + \frac{\partial \phi}{\partial x} \right) \frac{\partial \eta}{\partial x} \tag{13}$$

Making the assumption that the velocity perturbations produced by the airfoil in the flowing stream are small, since the airfoil is assumed very thin, $\frac{\partial \phi}{\partial x}$ can be neglected. As in classical thin-airfoil theory, the tangency (or surface) boundary condition is applied on the x-axis (y=0), rather than on the actual surface itself. The infinity condition requires

$$\nabla \phi \longrightarrow 0 \qquad \text{as } x,y \longrightarrow \infty \tag{14}$$

The Kutta condition requires the velocity to be finite at the trailing edge. This is accomplished by setting

$$\frac{\partial \phi}{\partial x} = 0 \qquad \text{at the trailing edge} \tag{15}$$

In order to keep ϕ unique, a branch cut is introduced into the flowfield. The potential jump across this cut is equal to the circulation, defined by

$$\Gamma = \int_{\partial\Omega} \bar{V} \cdot d\bar{s} \tag{16}$$

where $\bar{V}$ is the tangent velocity and $d\bar{s}$ is along the path of integration. Therefore across the cut

$$\Gamma = \phi^{+} - \phi^{-} \qquad \text{is enforced.} \tag{17}$$

The actual value of Γ is determined by enforcing the Kutta condition. The pressure coefficient from small perturbation theory is (Ref 13)

$$C_p \simeq -2 \frac{\partial \phi}{\partial x} \tag{18}$$

Due to the linearity of the Laplace equation, the solution for a particular airfoil shape can be determined from the sum of the solutions to the three subproblems; thickness, camber, and flat plate at angle of attack, as shown in Fig 2. The difference among the three problems is the treatment of the boundary condition on the airfoil (Ref 14). For the thickness problem

$$\left.\frac{\partial \phi}{\partial y}\right|_{0^{\pm}} = \pm \frac{\partial \eta_t}{\partial x} U_\infty \tag{19}$$

where

$$\eta_t = \frac{1}{2}(\eta_u - \eta_l) \tag{20}$$

and η_u = upper surface

η_l = lower surface

For the camber problem

$$\left.\frac{\partial \phi}{\partial y}\right|_{0^\pm} = \frac{\partial \eta_c}{\partial x} U_\infty \tag{21}$$

where

$$\eta_c = \frac{1}{2}(\eta_u + \eta_l) \tag{22}$$

The condition for a flat plate at angle of attack α is

$$\left.\frac{\partial \phi}{\partial y}\right|_{0^\pm} = -\alpha U_\infty \tag{23}$$

The Finite Element Approximation

The method of weighted residuals is used to obtain the finite element equations and an approximate solution to the Laplace equation (Ref 3). To apply the method ϕ is approximated by

$$\phi \simeq \tilde{\phi} = \sum_{i=1}^{N} N_i \phi_i \tag{24}$$

where N_i are assumed independent functions chosen such that all global boundary conditions are satisfied, ϕ_i are the unknown nodal parameters, and N is the number of system nodes. Since $\tilde{\phi}$ is an approximate solution, when substituted into the Laplace equation, it does not exactly satisfy the equation. The equation is thus set equal to an error,

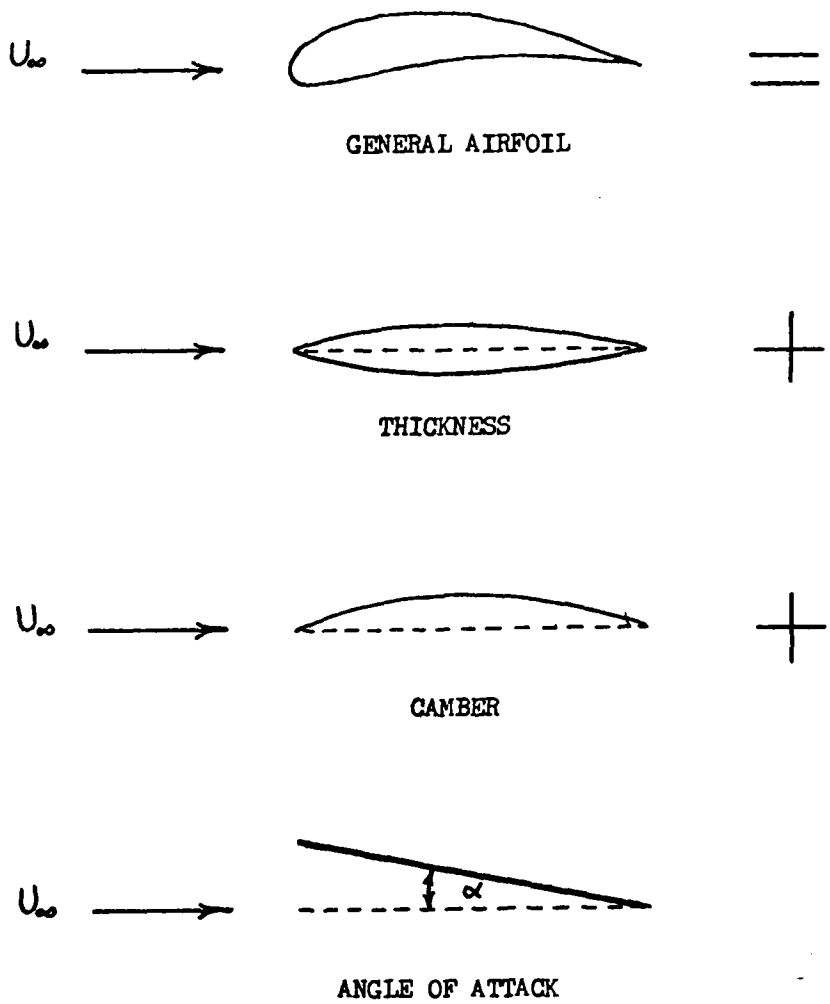

Figure 2. Airfoil Problem Superposition

$\mathcal{E}$. Thus

$$\nabla^2 \tilde{\phi} = \mathcal{E} \tag{25}$$

The method of weighted residuals attempts to determine the ϕ_i unknowns in such a way that the error over the solution domain is small. This is accomplished by forming a weighted average of the error and specifying that this weighted average vanishes over the solution domain. Thus

$$\iint_{\Omega} \nabla^2 \tilde{\phi} \, W_i \, d\Omega = 0 \tag{26}$$

where W_i are the linearly independent weighting functions. Equation (26) is integrated by parts to introduce the influence of the natural boundary conditions

$$\iint_{\Omega} \nabla \tilde{\phi} \cdot \nabla W_i \, d\Omega - \int_{\partial\Omega} \nabla \tilde{\phi} \cdot \bar{n} \, W_i \, d\partial\Omega \tag{27}$$

The weight functions W_i are set equal to the trial functions N_i (Galerkin's Method). Equation (27) becomes

$$\iint_{\Omega} \nabla \tilde{\phi} \cdot \nabla N_i \, d\Omega - \int_{\partial\Omega} \nabla \tilde{\phi} \cdot \bar{n} \, N_i \, d\partial\Omega = 0 \tag{28}$$

Since equation (28) holds for any point in the domain, it also holds for any group of points defining an arbitrary element e contained in the whole domain. Because of this, a local approximation can be made one element at a time, providing $\tilde{\phi}$ and N_i satisfy certain continuity requirements.

The trial function for each element can be denoted by

$$\phi^{(e)}(x,y) = N_j^{(e)}(x,y)\,\phi_j^{(e)} \tag{29}$$

Substituting into equation (28)

$$\iint_{\Omega} \nabla\phi^{(e)} \cdot \nabla N_i \, d\Omega - \int_{\partial\Omega^*} \nabla\phi^{(e)} \cdot \bar{n} \, N_i \, d\,\partial\Omega = 0 \tag{30}$$

where $*$ denotes that this integral is non-zero only for those elements that border the boundary of Ω. In matrix form, the element equations can be written as

$$K_{ij}^{(e)} \phi_j^{(e)} = f_i^{(e)} \tag{31}$$

where $K_{ij}^{(e)}$ is the elemental stiffness matrix, and $f_i^{(e)}$ is the element forcing vector.

The elemental $K_{ij}^{(e)}$ and $f_i^{(e)}$ matrices are described in Appendices A through C. The elemental equations are transformed into a global system of equations through an assembly procedure. The global system can be expressed as

$$K_{ij}\,\phi_j = F_i \tag{32}$$

<u>Treatment of Farfield Boundary</u>

In the finite element solution for the governing differential equation, the flowfield is discretized into a finite number of elements. Thus the infinite domain Ω is replaced by a finite domain Ω_F. There

are two possible techniques to treat the farfield boundary conditions (Ref 15).

The first method assumes that Ω_F is very large, and that the actual gradient boundary conditions, $\nabla\phi \rightarrow 0$, are enforced along $\partial\Omega_F$. This condition is substituted into the line integral term of the element equations (30). Solving the differential equation with this condition and the solid boundary condition on the airfoil (both Neumann boundary conditions) results in a non-unique solution. To obtain a unique solution, the value of ϕ must be specified at a minimum of one node.

The second method is to impose the condition $\phi = \phi_{FF}$ along the farfield boundary $\partial\Omega_F$. The values of ϕ_{FF} should ensure satisfaction of the infinity condition and be valid everywhere in the farfield. This method has the advantage of reducing the solution domain, and has commonly been utilized by others using finite element methods. The reduction is accomplished through partitioning of the global system of equations as follows

$$\left[\begin{array}{c|c} K_{aa} & K_{ab} \\ \hline K_{ba} & K_{bb} \end{array}\right] \left\{\begin{array}{c} \phi_a \\ \hline \phi_b \end{array}\right\} = \left\{\begin{array}{c} f_a \\ \hline f_b \end{array}\right\} \tag{33}$$

The vector $\{\phi_b\}$ is composed of the P nodal values of ϕ_{FF} which are computed from the expression for $\phi = \phi_{FF}$. The vector $\{\phi_a\}$ is composed of the remaining M=N-P unknown nodal values of ϕ, which are determined from equation (33) by inverting matrix $[K_{aa}]$ resulting in

$$\{\phi_a\} = [K_{aa}^{-1}]\left(\{f_a\} - [K_{ab}]\{\phi_b\}\right) \tag{34}$$

The method used in this report was the first. The uniqueness of the flowfield was established through specification of the circulation.

III Solution Methods

Three different problem solution methods, involving different aspects of treating the branch cut were used to solve the flat-plate lifting problem.

Superposition

The first method used was developed by de Vries and Norrie (Ref 7). In this method, the velocity potential is defined as a superposition of a thickness problem and a lifting problem expressed by

$$\phi = \Gamma \phi_1 + \phi_2 \tag{35}$$

where Γ is the circulation, ϕ is the perturbation potential, ϕ_1 and ϕ_2 are the perturbation potentials of the subproblems. The two subproblems are solved as two separate boundary value problems stated:

a)

$$\begin{aligned} &\nabla^2 \phi_1 = 0 && \text{in } \Omega \\ &\frac{d\phi_1}{dn} = 0 && \text{on surface of airfoil} \\ &\frac{d\phi_1}{dn} = 0 && \text{on farfield boundary} \\ &(\phi_1)_U = 1 \qquad (\phi_1)_L = 0 \end{aligned} \tag{36}$$

where $(\phi_1)_U$ are the potentials of the top branch cut nodes, and $(\phi_1)_L$ are the potentials of the bottom branch cut nodes.

b)

$$\nabla^2 \phi_2 = 0 \qquad \text{in } \Omega$$

$$\frac{d\phi_2}{dn} = 0 \qquad \text{on the farfield boundary}$$

$$\frac{d\phi_2}{dn} = \frac{\partial \eta}{\partial x} \qquad \text{on the surface} \tag{37}$$

$$(\phi_2)_U = 0 \qquad (\phi_2)_L = 0$$

By differentiating equation (35) with respect to x, the x-component of velocity, u , is obtained.

$$u = \Gamma u_1 + u_2 \tag{38}$$

where u is the total x-component velocity, u_1 is the x-component velocity of ϕ_1 field, and u_2 is the x-component velocity of ϕ_2 field.

The Kutta condition is applied at the trailing edge by setting the total x-component velocity equal to zero there. The circulation can then be determined by equating equation (38) to zero, thus

$$\Gamma u_{1(TE)} + u_{2(TE)} = 0 \tag{39}$$

therefore,

$$\Gamma = - \frac{u_{2(TE)}}{u_{1(TE)}} \tag{40}$$

Once Γ is determined, its value along with the computed values for ϕ_1 and ϕ_2 can be combined in equation (35) to determine the total perturbation potential field. In this method, the u velocity along

the branch cut is constant. An advantage of this method is that the circulation is easily determined as a result of combining ϕ_1 and ϕ_2. Another advantage is that the stiffness matrix for both ϕ_1 and ϕ_2 are symmetric and banded storage and solution methods are applicable. A Gaussian elimination method was used to solve the system equations.

Iterative Method 1

In this method of solving the flat-plate problem, the finite element equations were modified for the jump in ϕ across the branch cut by setting

$$\phi_U = \frac{1}{2}\Gamma$$
$$\phi_L = -\frac{1}{2}\Gamma \tag{41}$$

and iterating the solution through the value of circulation until the u velocity at the trailing edge becomes zero. This method treats the flowfield as one boundary value problem, and requires solution of the finite element equations for each iteration of Γ. The same solution routine as previously noted was used. The stiffness matrix is again symmetric and banded, thus allowing the reduced storage method. As in the first method, the u velocity component along the branch cut is constant.

Iterative Solution Method 2

In this method, the flowfield is treated as one boundary value problem with the finite element equations modified for the jump in potential ϕ across the branch cut by defining

$$\phi_U - \phi_L = \Gamma \tag{42}$$

where the value of Γ is again determined through an iterative process as in the previous method. An additional constraint is added at the trailing edge to make the average velocity there equal to zero,

$$V_U + V_L = 0 \tag{43}$$

The requirements of equations (42) and (43) make the stiffness matrix non-symmetric, and thus the reduced storage methods used in the previous methods cannot be used. This problem was solved again using a Gaussian elimination method. The u velocity along the branch cut; however, is no longer required by the problem to be zero.

IV The Flat-Plate at Angle of Attack

The finite element results are presented for a flat-plate airfoil at a small angle of attack. The pressure coefficient distribution over the airfoil is determined using the solutions for the potential functions. Appendices A through C contain the computational details of how this is done. The calculated pressure distributions are compared to the results from classical thin-airfoil theory. The value of circulation, obtained as a consequence of applying the Kutta condition, is also compared to the thin-airfoil theory value.

Three types of elements were used to obtain the pressure coefficient distribution: linear, Appendix A; mixed, Appendix C; and quadratic, Appendix B. The effect of the farfield boundary location and refinement of the element discretization in the flowfield domain was determined for each element. The superposition method was used to generate the results in this section; however, the iterative solution methods were shown to produce the same results.

Flowfield Grid Parameters

An automatic mesh generation technique was used to produce the nodal coordinates. The parameters of the grids were as follows:

YMAX - the y-direction width of the rectangular field, with the airfoil approximated at $y=0$.

XMAX - the x-direction width of the rectangular field.

NDX - the number of divisions in the x-direction in the farfield, NDX/2 in front of and behind the airfoil. The value of NDX is equivalent to one element for linear and half an element for quadratic elements.

NDXA - the number of x-direction divisions along the airfoil surface. The same relationship with respect to elements as in the NDX parameter.

NDY - the number of y-direction divisions in the flowfield. The same relationships to elements as in the x-direction parameters.

Linear Elements

For linear elements, the u velocity along the airfoil surface and element boundary interface is constant for each element, reference Appendix A. For this reason, applying the Kutta condition at the trailing edge requires the velocity and as a consequence the pressure coefficient to be zero in the last element on the top and bottom of the airfoil. This requirement can produce a significant error at the trailing edge, if the last element is large with respect to the airfoil.

Three grid patterns were used: a uniformly spaced grid, Fig 3; a uniform grid with a small (.005 chord) element at the trailing edge, Fig 4; and a grid in which the size of the elements increases exponentially from the leading and trailing edges, in both the x- and y-directions over the airfoil and in the field, Fig 5.

Farfield Boundary Location.

As previously noted, the location of the farfield boundary is characterized by the parameters XMAX and YMAX. The solution of the problem could be obtained for any combination of these two parameters; however, it is desireable to reduce the computation time and space by selecting the smallest possible area. The method used was that used by Marsh (Ref 15). The lower bounds on these two parameters, XMAX and YMAX, were determined from a series of solutions for elements of fixed size.

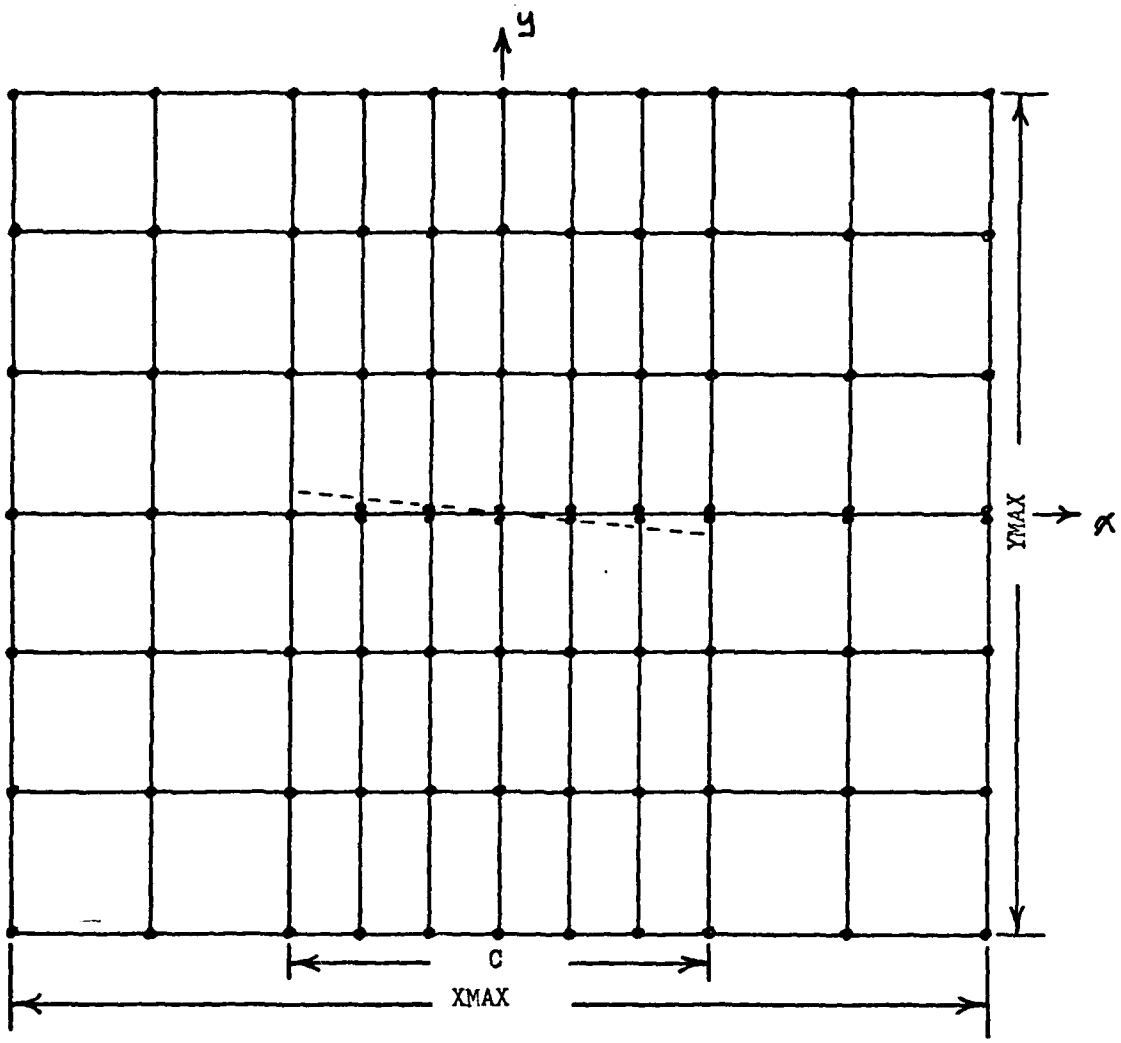

Figure 3. Linear Equally Spaced Element Discretization

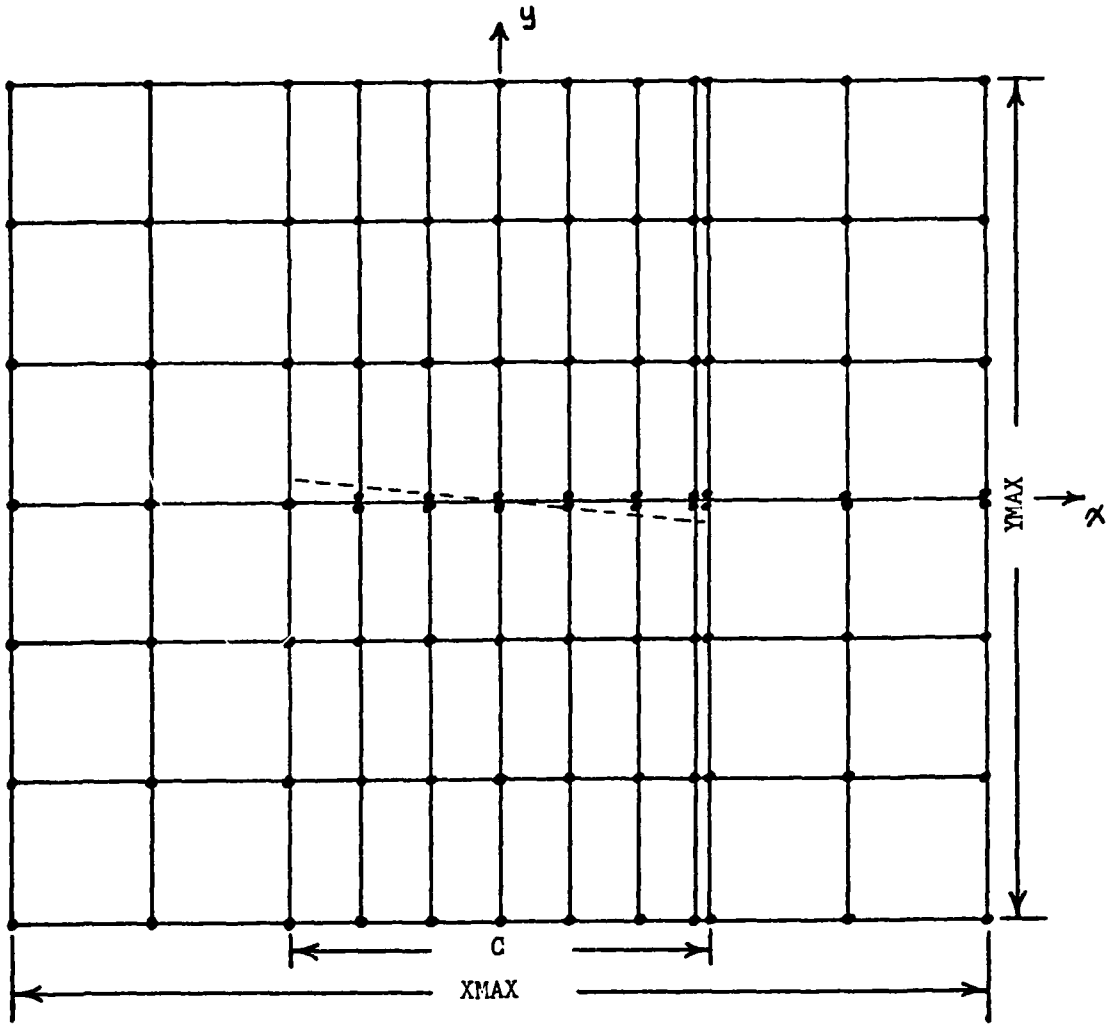

Figure 4. Linear Equally Spaced Element Discretization With Small Trailing Edge Element

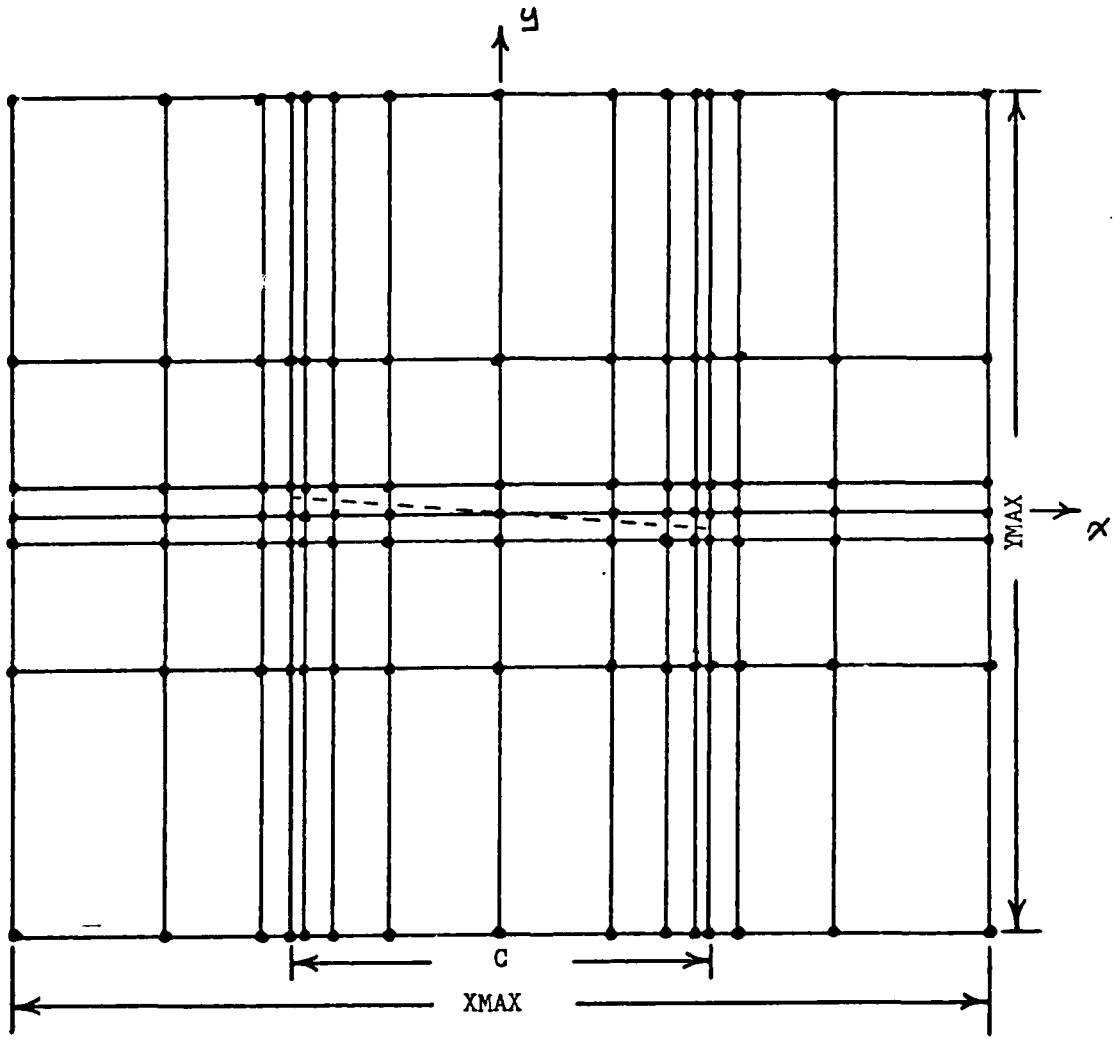

Figure 5. Linear Exponentially Spaced Element Discretization

This fixed size, or Aspect Ratio (AR), is the ratio of $\Delta x/\Delta y$ of the element. This analysis was accomplished with the equally spaced grid with small trailing edge element. Although this small element is not the same size as the others, it actually has a beneficial result, as will be seen later. A base solution for relatively small values of XMAX and YMAX, with constant AR for the elements was first established. The size of the field was then expanded on the outer perimeter of the flow domain. A series of solutions was thus obtained for increasing values of XMAX and YMAX. By holding the element size constant and varying only the number of elements, the effect of the farfield boundary location on the pressure distribution can be determined. The base flowfield was first expanded in the x-direction only, keeping the number of y-direction elements constant. The results of this expansion are shown in Fig 6. These results indicate that there is no change in the circulation for XMAX greater than 2.5 chordlengths. The flowfield was next expanded in the y-direction, holding XMAX= 2.5c. The results of this expansion are shown in Fig 7. It is seen from these results that a YMAX greater than 3.0c produces no change in the circulation. It can; therefore be concluded that a farfield boundary location greater than XMAX= 2.5c and YMAX= 3.0c has no effect on the pressure distribution on the airfoil.

Pressure Coefficient.

The effect of the three types of grids on the pressure distribution was investigated next. The value of the circulation being proportional to the integrated pressure distribution can be used as a measure of the relative accuracy of the pressure distribution, in an average sense. In Fig 8, the three grids are compared with respect to the convergence of the circulation to the classical thin-airfoil theory value, when

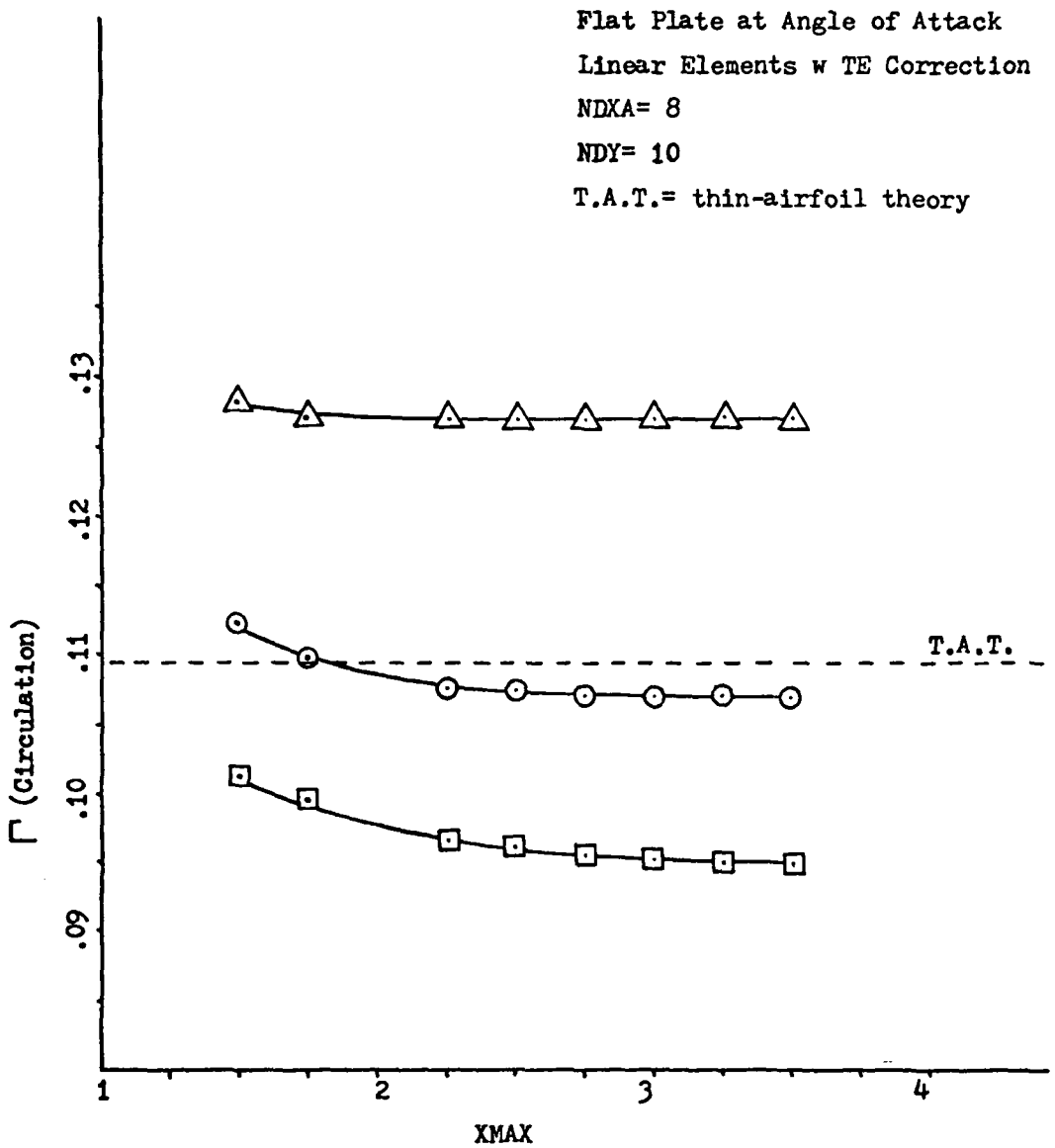

Symbol	AR	YMAX
△	1.00	1.25
⊙	0.50	2.5
⊡	0.25	5.0

Figure 6. Linear Elements, Constant Aspect Ratio, Expansion of Domain in x-direction

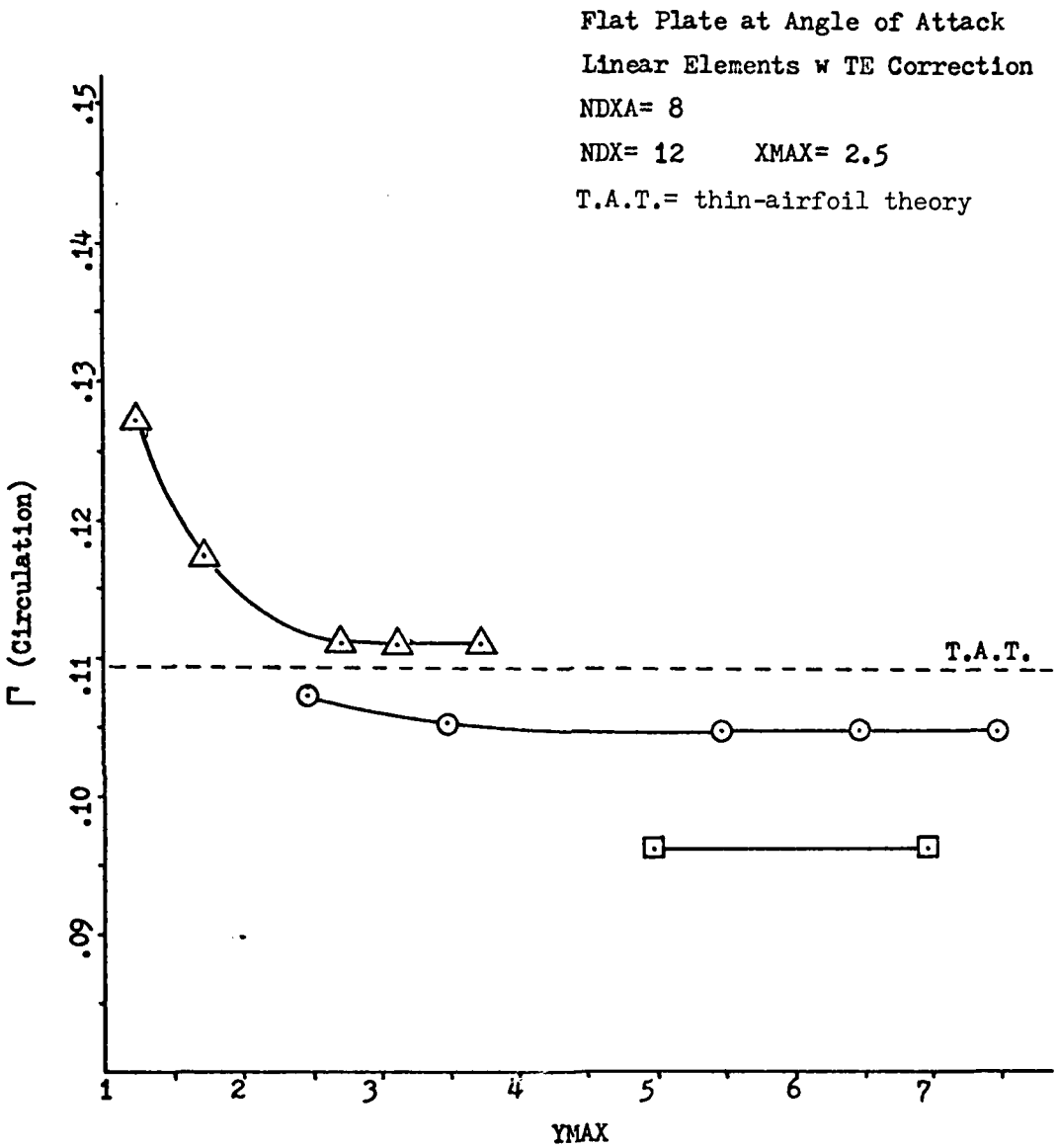

Symbol	AR
△	1.00
⊙	0.50
⊡	0.25

Figure 7. Linear Elements, Constant Aspect Ratio, Expansion of Domain in y-direction

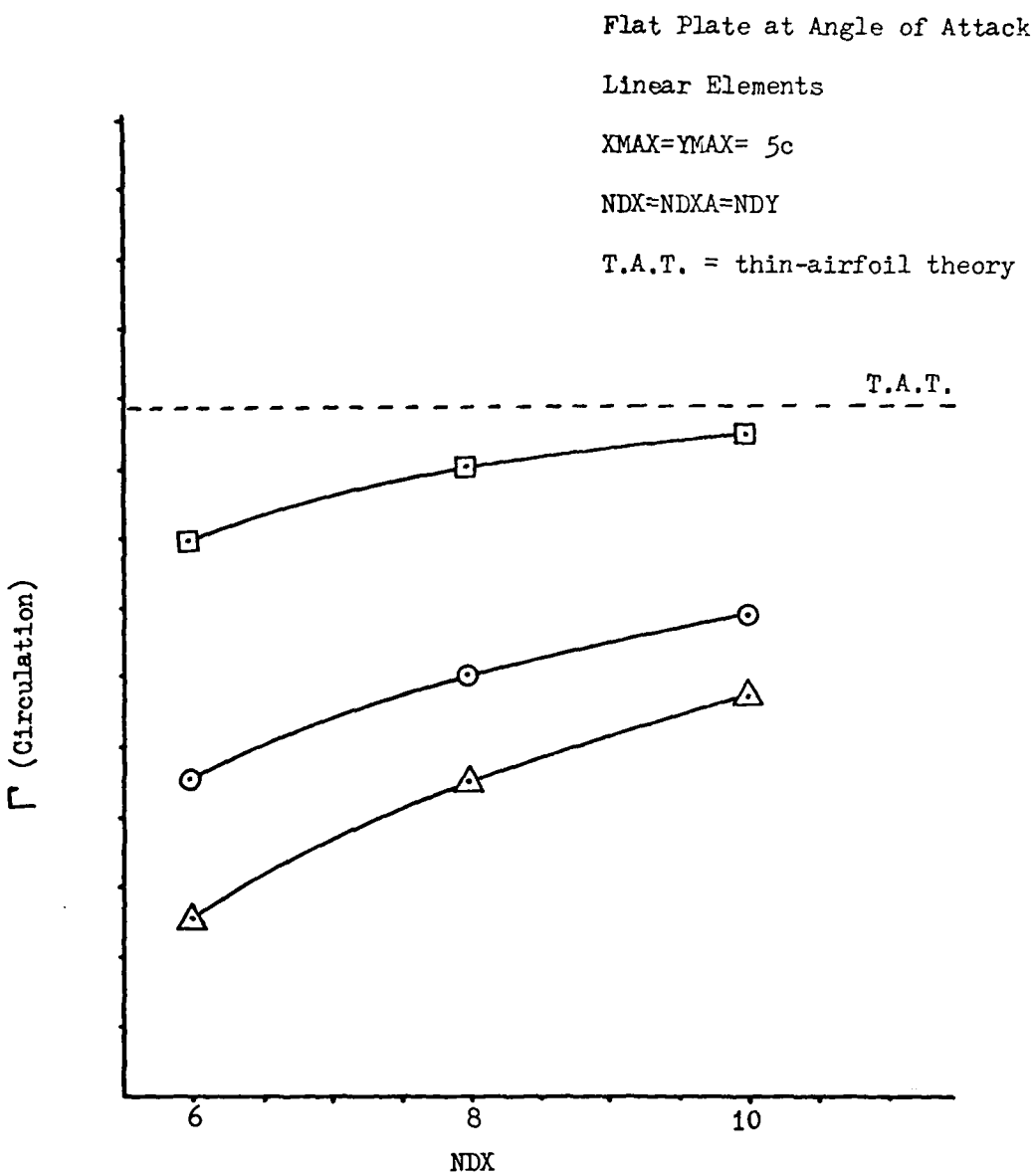

Symbol	Grid
△	Linear Elements - Uniformly Spaced
⊙	Linear Elements - with small TE element
⊡	Linear Elements - Exponential Spacing

Figure 8. Convergence of Circulation For Linear Element Grids

a uniform reduction in grid size is made. From this figure, it is seen that the equally spaced grid is the slowest of the three to converge. An examination of the actual pressure distribution in Fig 9 shows that the zero pressure requirement in the last element, to impose the Kutta condition, effectively shortens the airfoil by the width of that element. The decrease in width of the airfoil surface elements can improve this condition; however, since the size of this last element is inversely proportional to the number of elements, it would take 20 elements to extend to 95% of chord and 200 elements to cover 99.5% of chord. From Fig 8, it is seen that introducing the small element at the trailing edge improves the convergence of the equally spaced element grid. The pressure distribution for this case is shown in Fig 10. In this case 99.5% of the airfoil is covered by non-zero elements, for any desired number of surface elements. Comparing Figs 9 and 10, it can be seen that since the grid with the trailing edge element is effectively longer, for the same grid parameters, all values of the pressure distribution are slightly higher in each interval. The third grid, exponentially spaced, is shown in Fig 8 to be the best of the three. The 200 element grid, corresponding to NDX = NDY = NDXA = 10, has a circulation value only 2.2% below that of the exact solution, while the first two grids with these same parameters are 19.3% and 14.1% respectively below the exact. The pressure distribution for the exponential grid case is shown in Fig 11. The major reason for the improvement in circulation is the concentration of smaller elements near the leading and trailing edges. The small elements at the leading edge allow for a better approximation to the singularity, while at the trailing edge they automatically reduce the size of the zero pressure element. The large elements near the

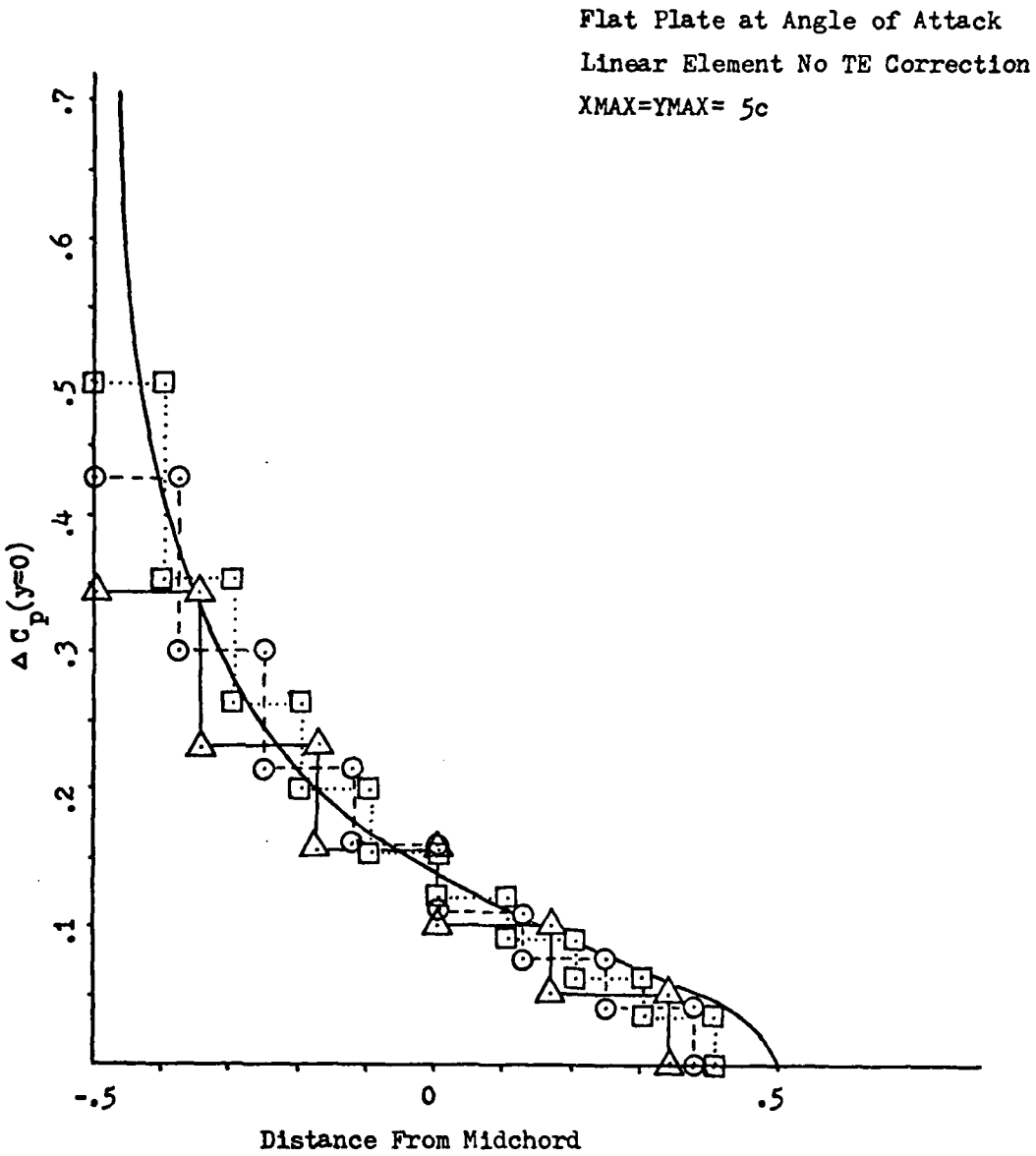

Symbol	Nodes	Elements	NDX	NDXA	NDY
△	100	72	6	6	6
⊙	165	128	8	8	8
⊡	246	200	10	10	10

Figure 9. Pressure Distribution For Linear Equally Spaced Elements and Uniform Reduction of Element Size

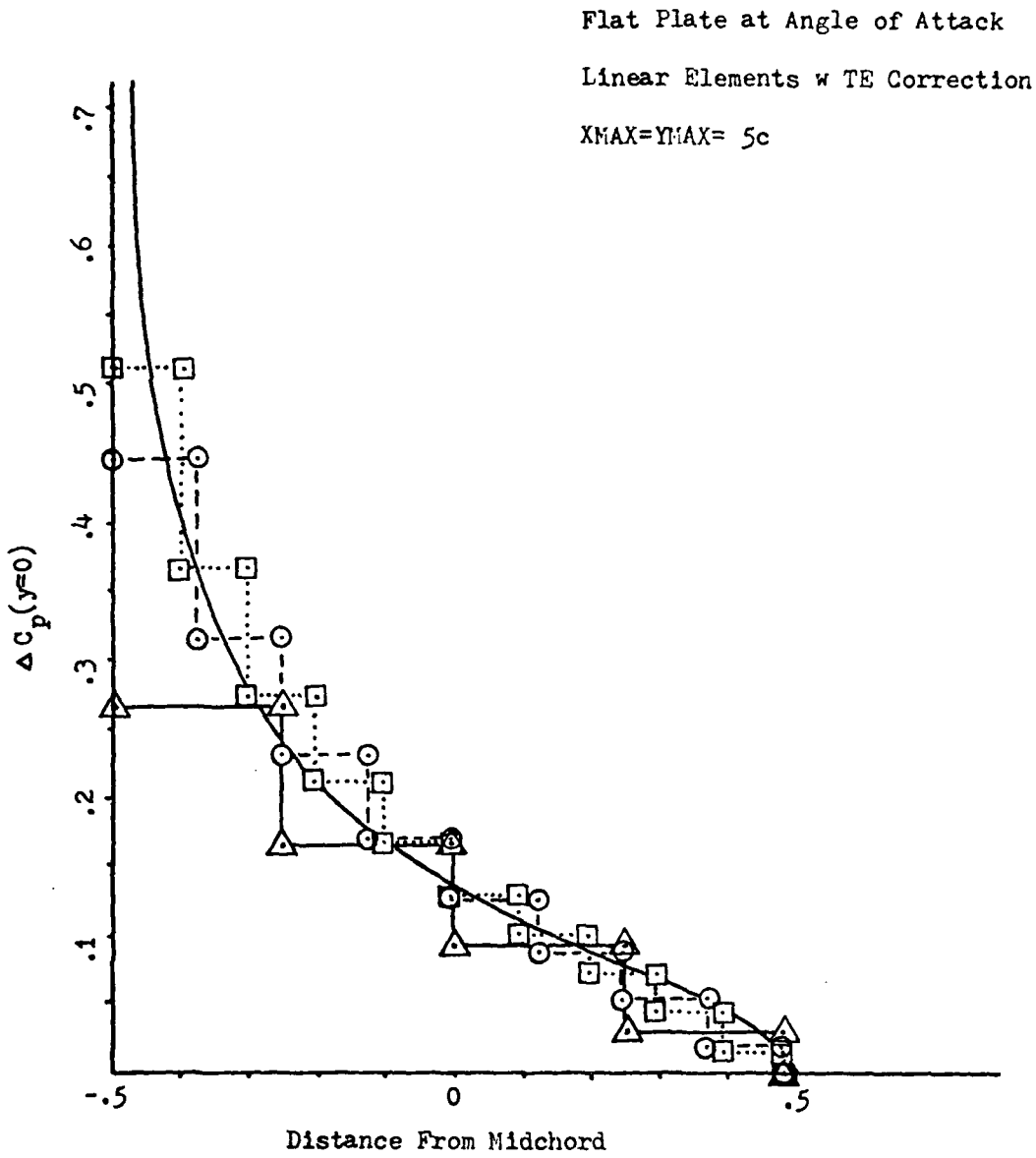

Symbol	Nodes	Elements	NDX	NDXA	NDY
△	57	36	4	4	4
⊙	175	136	8	8	8
⊡	258	210	10	10	10

Figure 10. Pressure Distribution For Linear Equally Spaced Elements With Small Trailing Edge Element and Uniform Reduction of Element Size

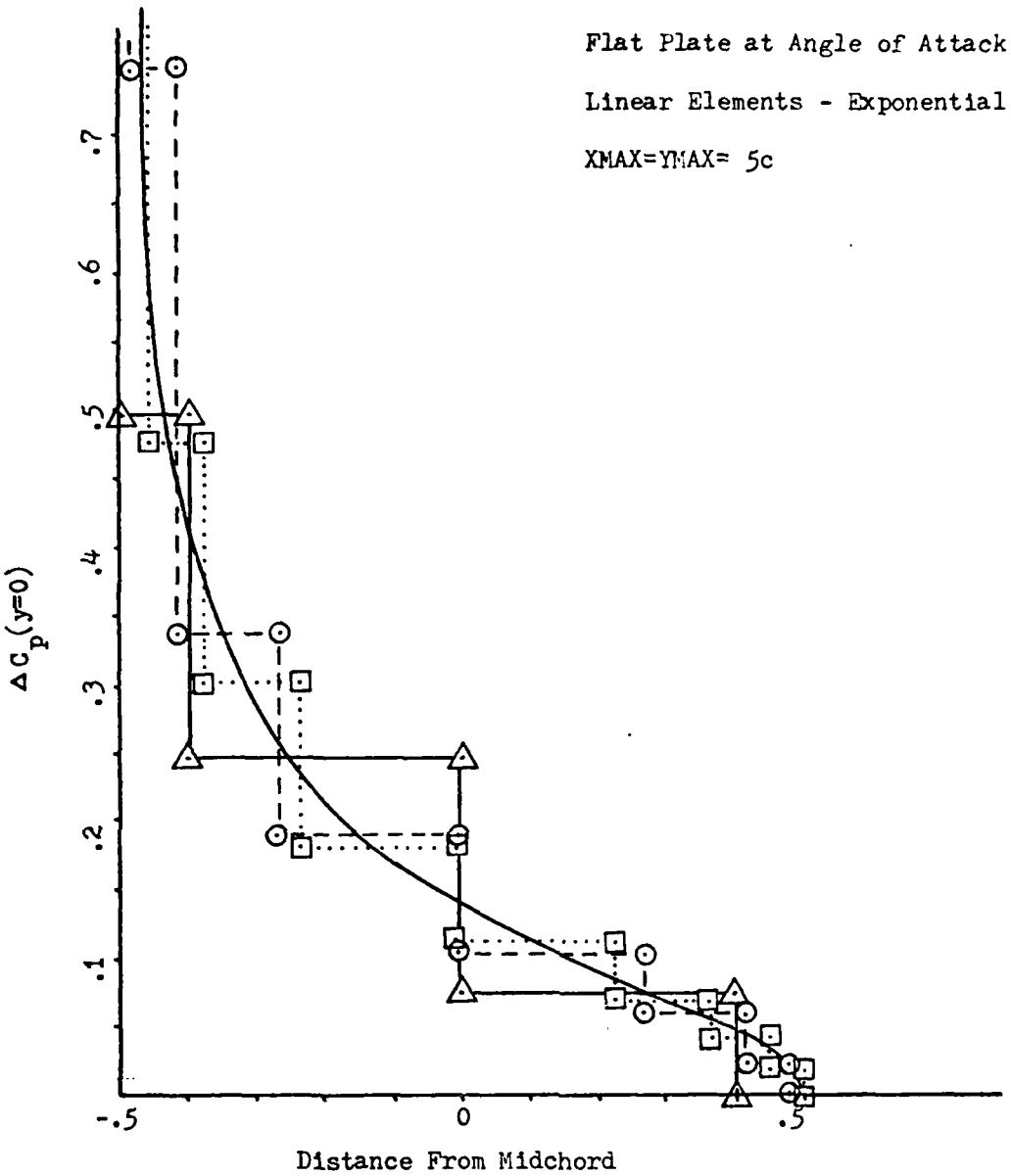

Symbol	Nodes	Elements	NDX	NDXA	NDY
△	51	32	4	4	4
⊙	165	128	8	8	8
⊡	246	200	10	10	10

Figure 11. Pressure Distribution For Linear Exponentially Spaced Elements and Uniform Reduction of Element Size

midchord do not cause a significant error, as this portion of the exact curve is the most linear. In all three cases the pressure distribution step function approximately intersects the exact solution at some point in the interval. Thus, even coarse grids are not unrealistic in approximating the pressure distribution. In Figs 9-11, the effect of uniformly reducing the element size on the pressure distribution is shown. The fastest convergence occurs at the midchord and the slowest occurs at the leading edge singularity. The solution trend in all cases is correct, in that they approach the exact solution as the element size is made smaller. Refinement of the elements through the farfield parameters, NDX and NDY, are shown in Figs 12-14 for the three grids. This technique produces a fast convergence from midchord to the trailing edge, and slower convergence toward the leading edge. Refinement of the elements through the airfoil element width parameter NDXA only is shown in Figs 15-17 for the three grids. This refinement exhibits slower convergence at the leading edge than the previous method; however, this method shows better convergence to the shape of the exact curve.

These refinement techniques, suggest the best method of refinement would be to first refine the farfield parameters until the leading edge element pressure varies little with further refinement, and then refine through the surface element parameter NDXA to obtain the best approximation to the exact curve.

Mixed Elements

In order to eliminate the step function characteristic of the pressure distribution for the previous linear element grids, a mixed element was introduced along the airfoil surface, Fig 18, with the quadratic side aligned along the airfoil boundary. Refer to Appendix C

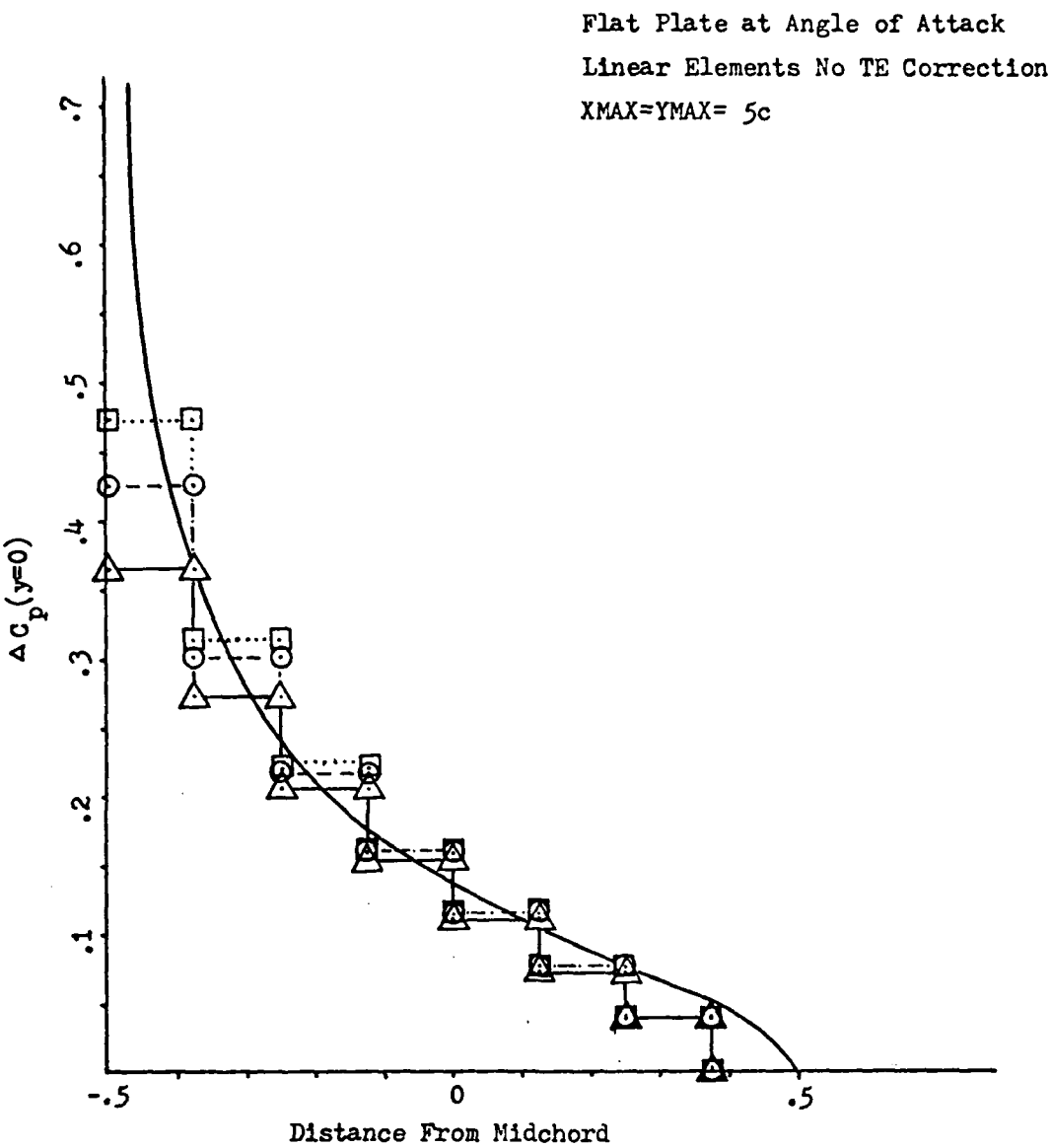

Symbol	Nodes	Elements	NDX	NDXA	NDY
△	116	84	6	8	6
⊙	165	128	8	8	8
⊡	222	190	10	8	10

Figure 12. Pressure Distribution For Linear Equally Spaced Elements and Uniform Reduction of Farfield Parameters Only

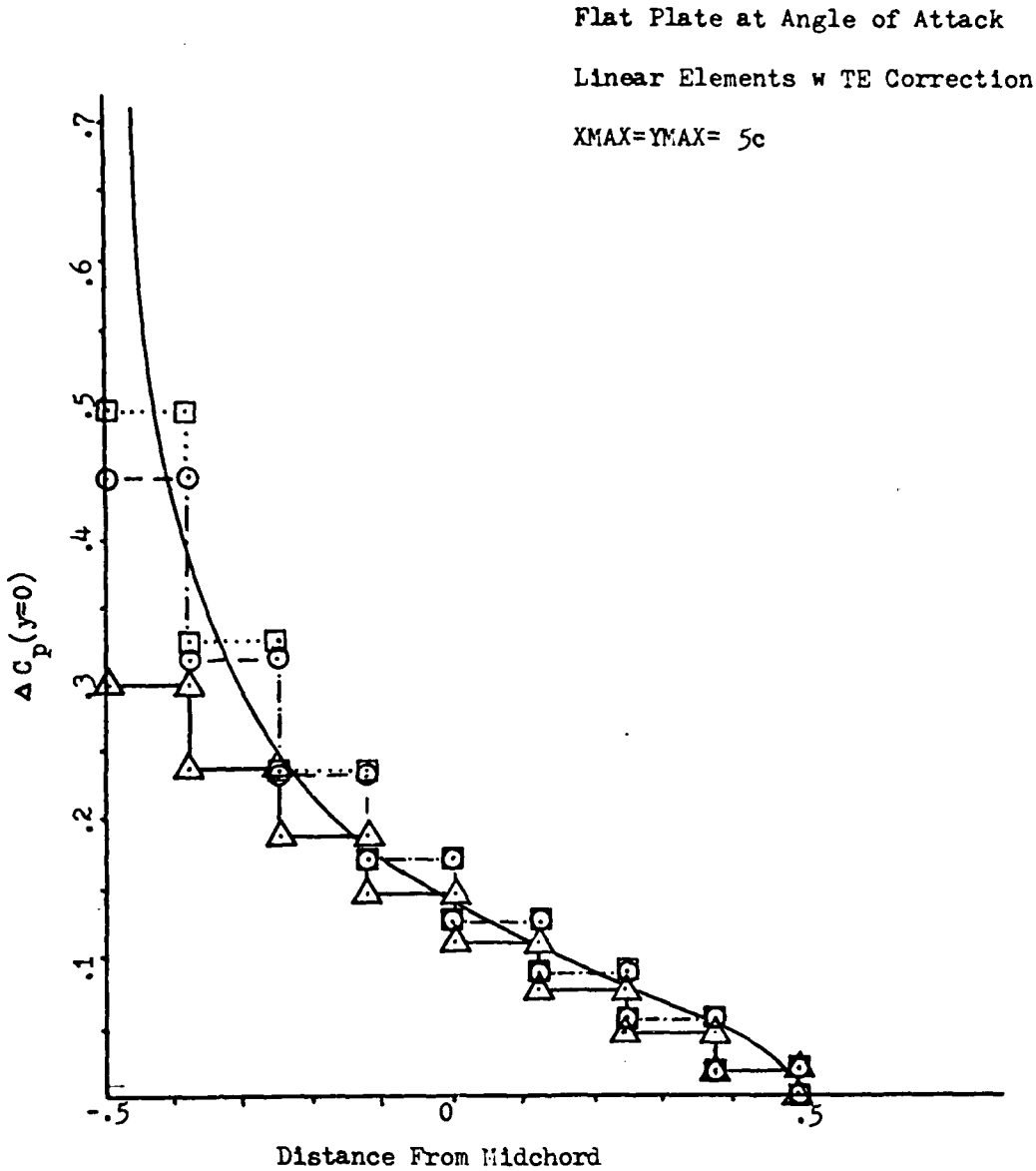

Symbol	Nodes	Elements	NDX	NDXA	NDY
△	81	52	4	8	4
⊙	175	136	8	8	8
⊡	234	190	10	8	10

Figure 13. Pressure Distribution For Linear Equally Spaced Elements With Small Trailing Edge Element and Uniform Reduction of Farfield Parameters Only

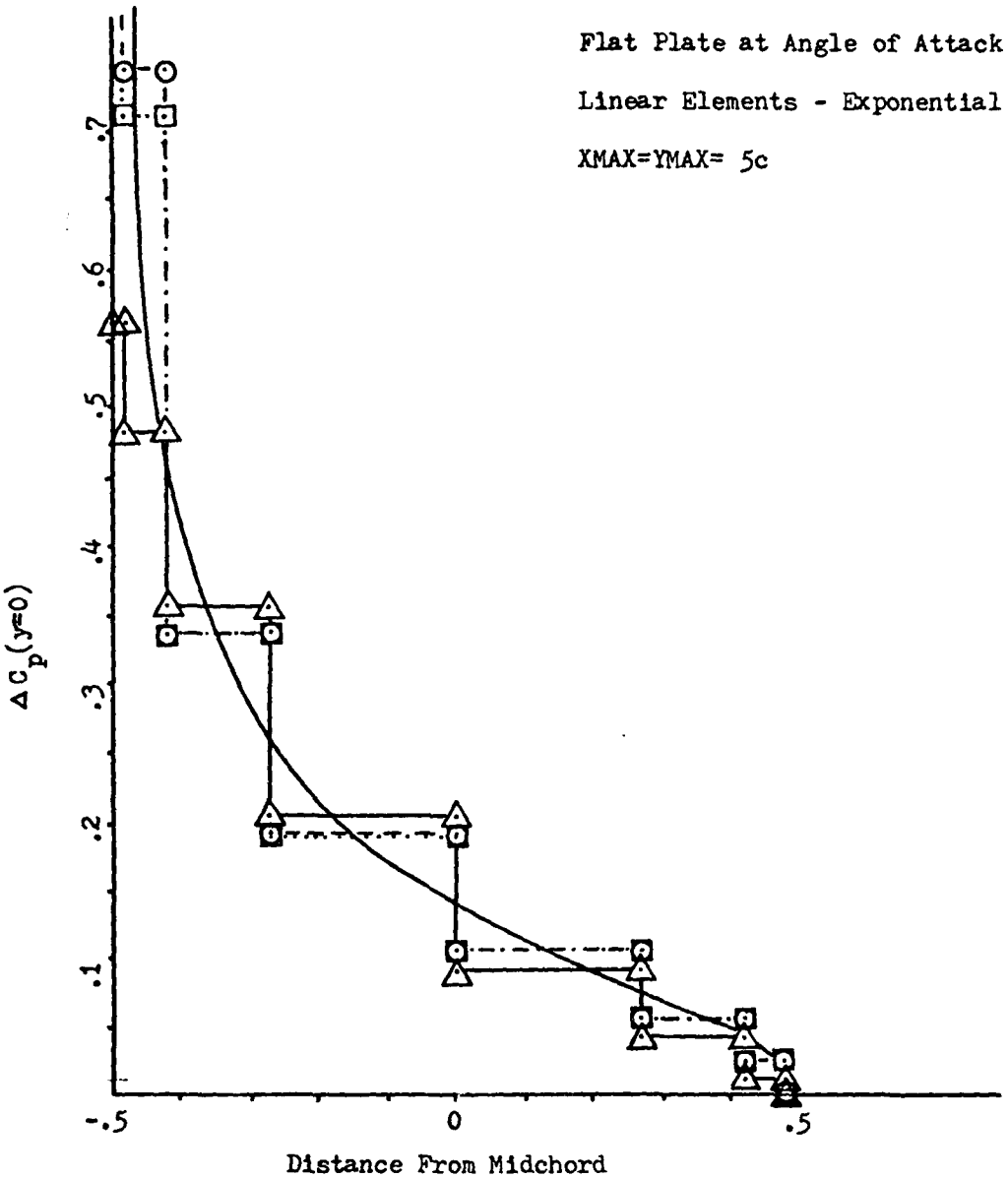

Symbol	Nodes	Elements	NDX	NDXA	NDY
△	75	48	4	8	4
⊙	165	128	8	8	8
⊡	222	180	10	8	10

Figure 14. Pressure Distribution For Linear Exponentially Spaced Elements and Uniform Reduction of Farfield Parameters Only

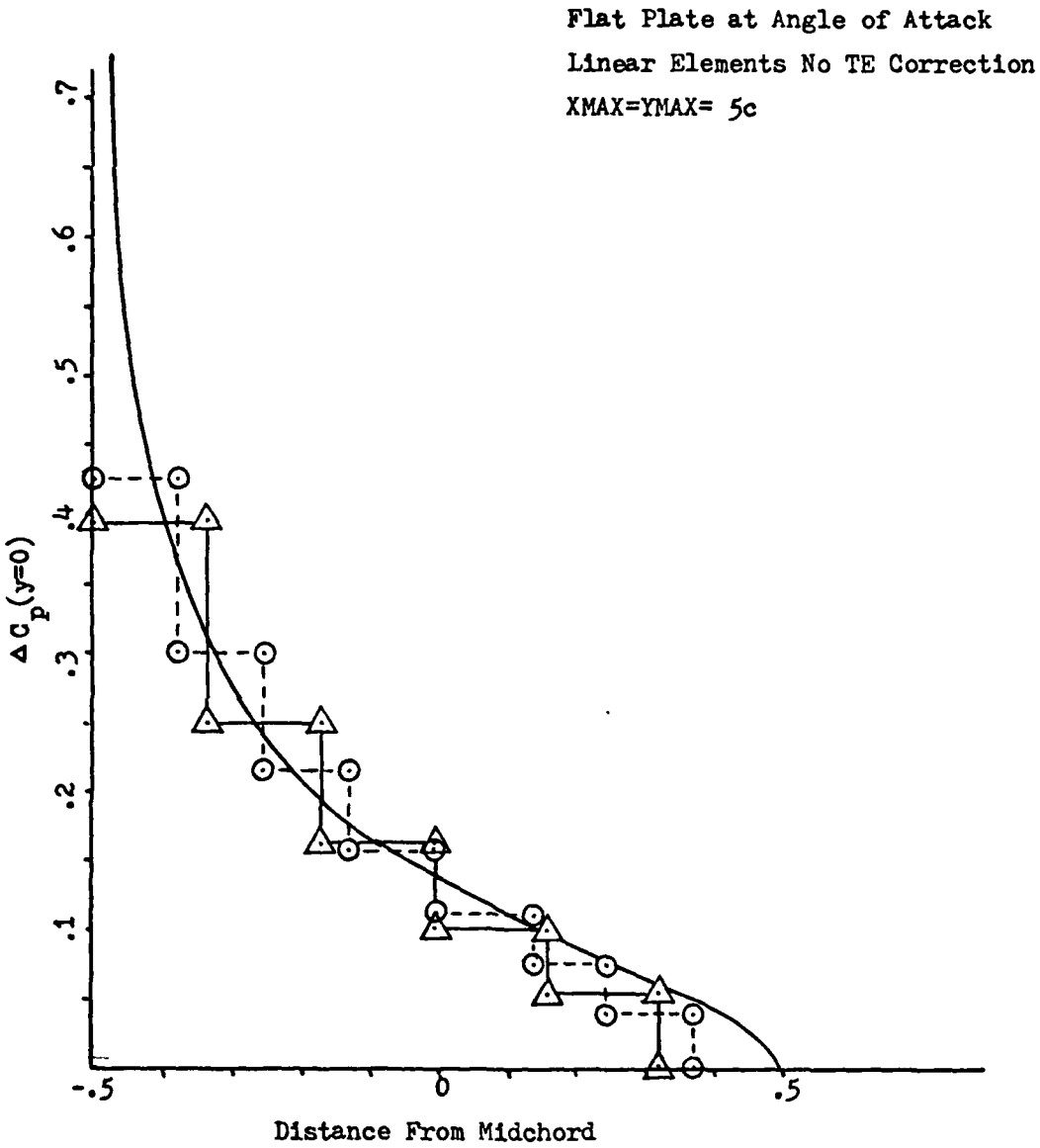

Symbol	Nodes	Elements	NDX	NDXA	NDY
△	145	112	8	6	8
⊙	165	128	8	8	8

Figure 15. Pressure Distribution For Linear Equally Spaced Elements and Uniform Reduction of Airfoil Element Width Parameter

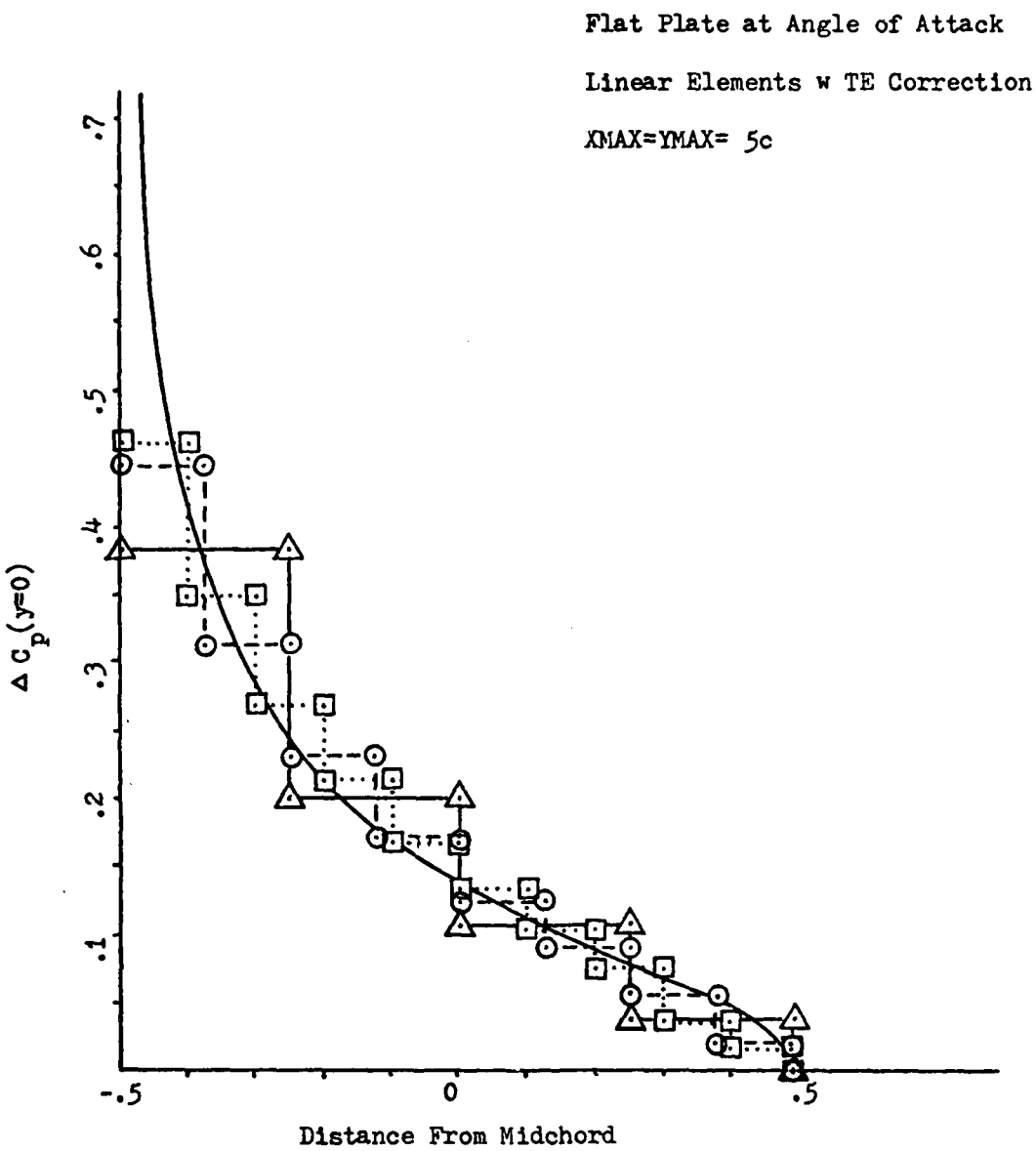

Symbol	Nodes	Elements	NDX	NDXA	NDY
△	135	104	8	4	8
⊙	175	136	8	8	8
⊡	195	152	8	10	8

Figure 16. Pressure Distribution For Linear Equally Spaced Elements With Small Trailing Edge Element and Uniform Reduction of Airfoil Element Width Parameter

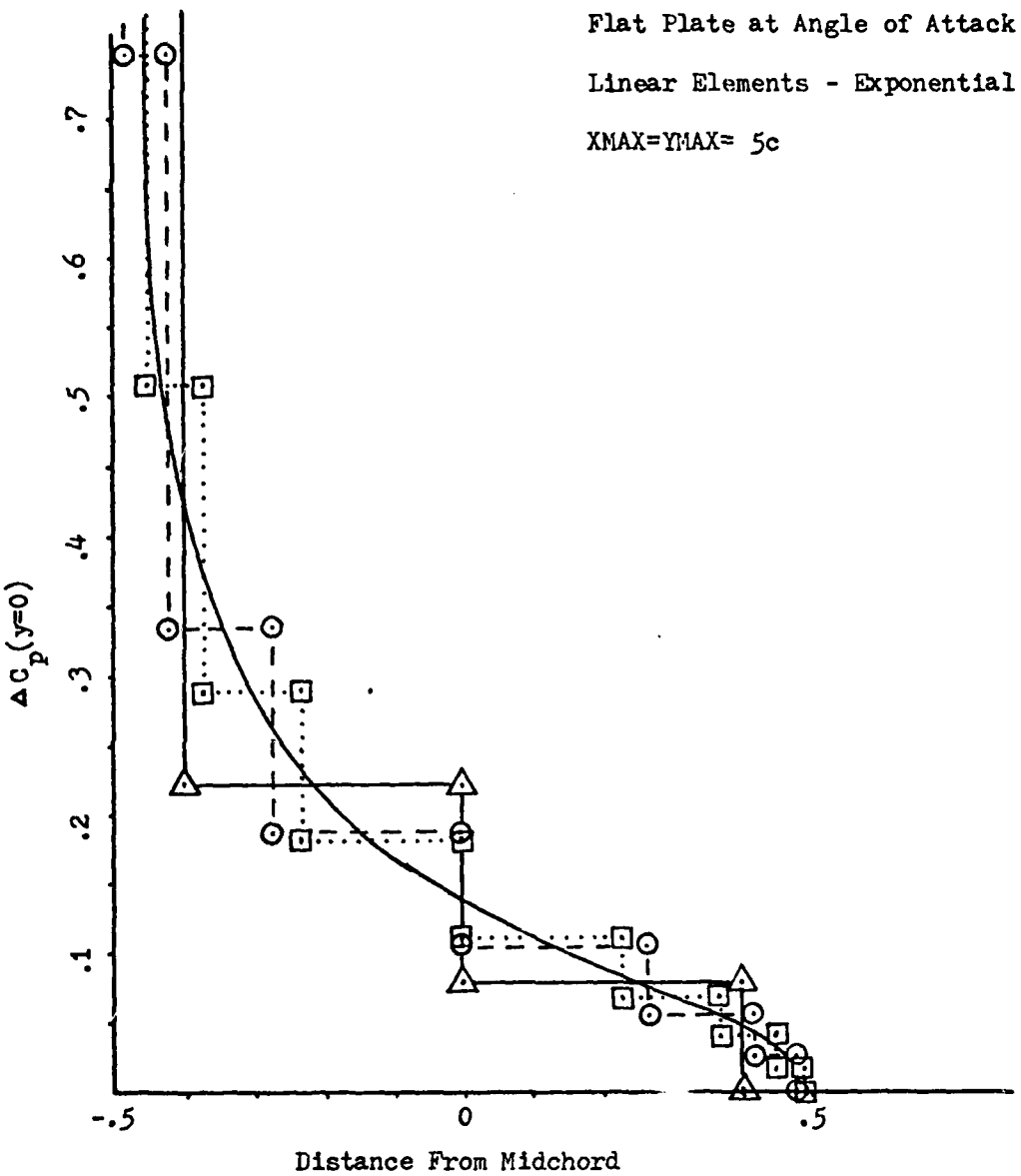

Symbol	Nodes	Elements	NDX	NDXA	NDY
△	125	96	8	4	8
⊙	165	128	8	8	8
⊡	185	144	8	10	8

Figure 17. Pressure Distribution For Linear Exponentially Spaced Elements and Uniform Reduction of Airfoil Width Parameter

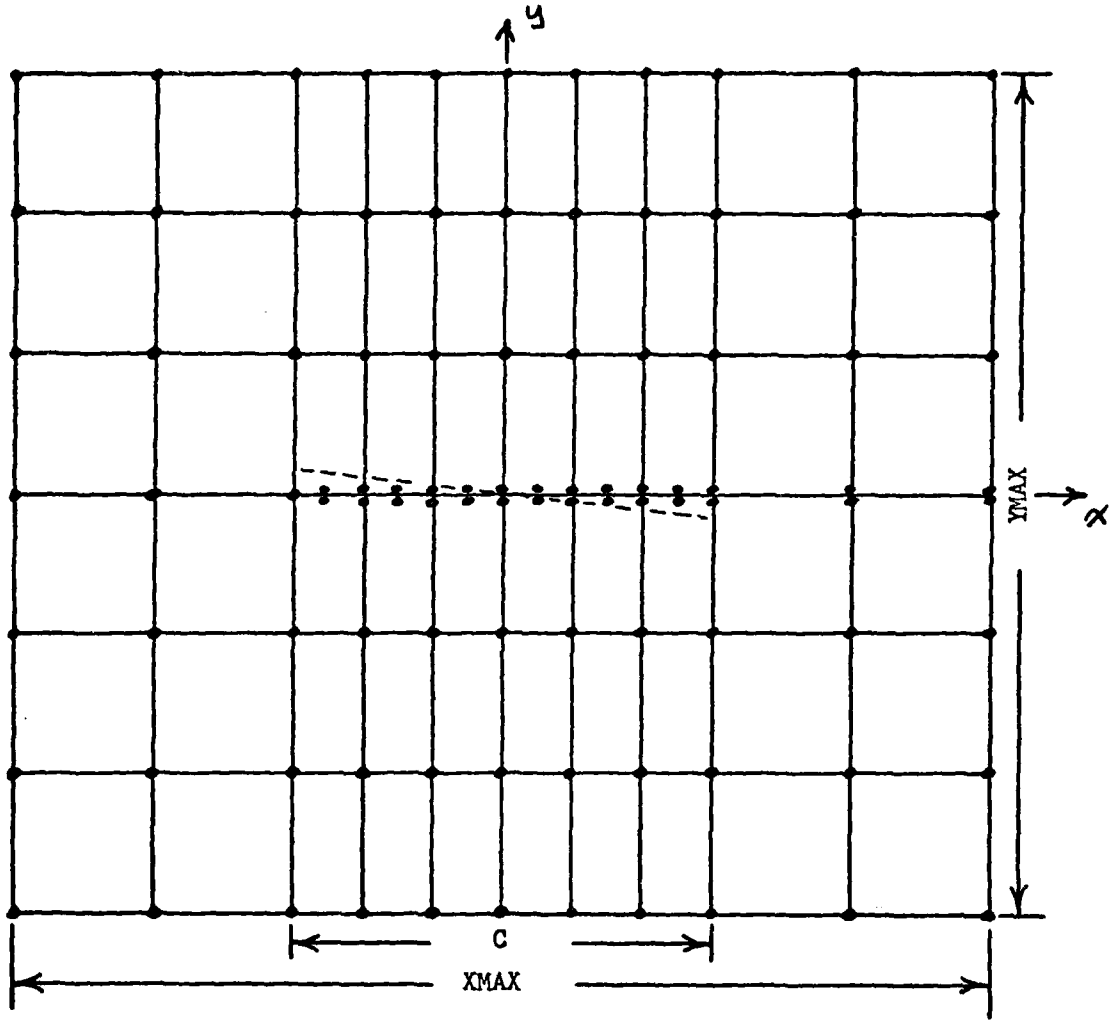

Figure 18. Mixed Element Discretization

for formulation of equations with this element. With this modification the velocity and as a consequence the pressure along the airfoil surface is a linear function in each element, rather than a constant. This allows the application of the Kutta condition at the last node on the airfoil rather than the entire last element as done previously. Thus the mixed element prevents the shortened airfoil effect that occurs when linear elements are used.

Farfield Boundary Location.

The procedures used for determining the farfield boundary location in the linear element section were also used for the mixed elements. The results of expanding the field in the x-direction are shown in Fig 19, while the subsequent expansion in the y-direction is shown in Fig 20. It can; therefore, be concluded that a farfield boundary location greater than XMAX= 2.5c and YMAX= 3.5c has no effect on the pressure distribution on the airfoil.

Pressure Coefficient.

The effect of element size on the pressure coefficient distribution and circulation were accomplished like that for linear elements. The comparison of the convergence to the thin-airfoil theory value of circulation with those of the two equally spaced grids in the previous section are shown in Fig 21. From this figure it is seen that the mixed elements on the airfoil effectively produce the same circulation as the grid with the small trailing edge correction element. Thus the mixed elements automatically correct for the trailing edge error that was seen to be a problem for the equally spaced grid in the previous section. The pressure distribution for the uniform reduction in element size is shown in Fig 22. When this distribution is compared with that for the

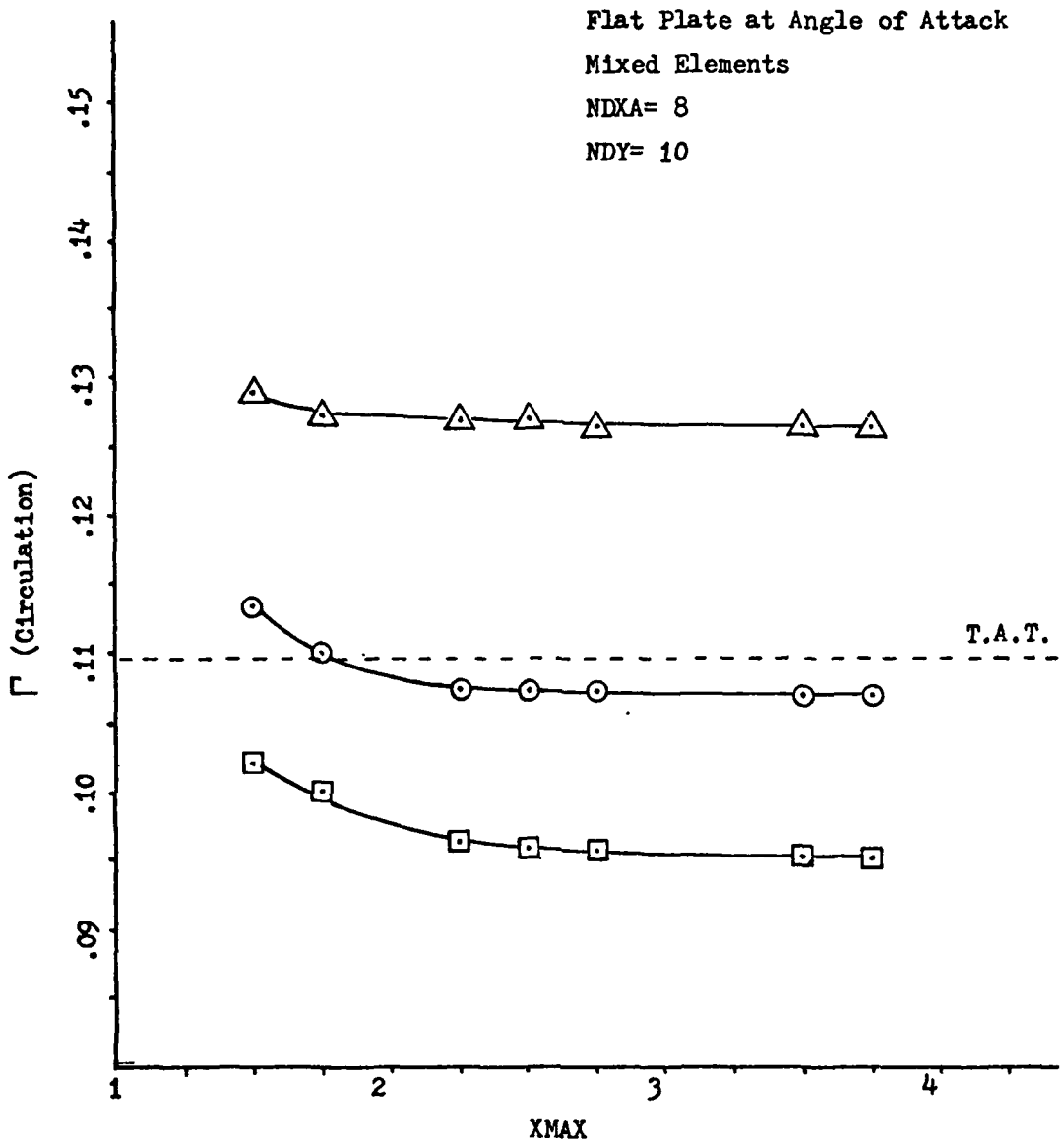

Symbol	AR	YMAX
△	1.00	1.25
⊙	0.50	2.5
⊡	0.25	5.0

Figure 19. Mixed Elements, Constant Aspect Ratio, Expansion of Domain in x-direction

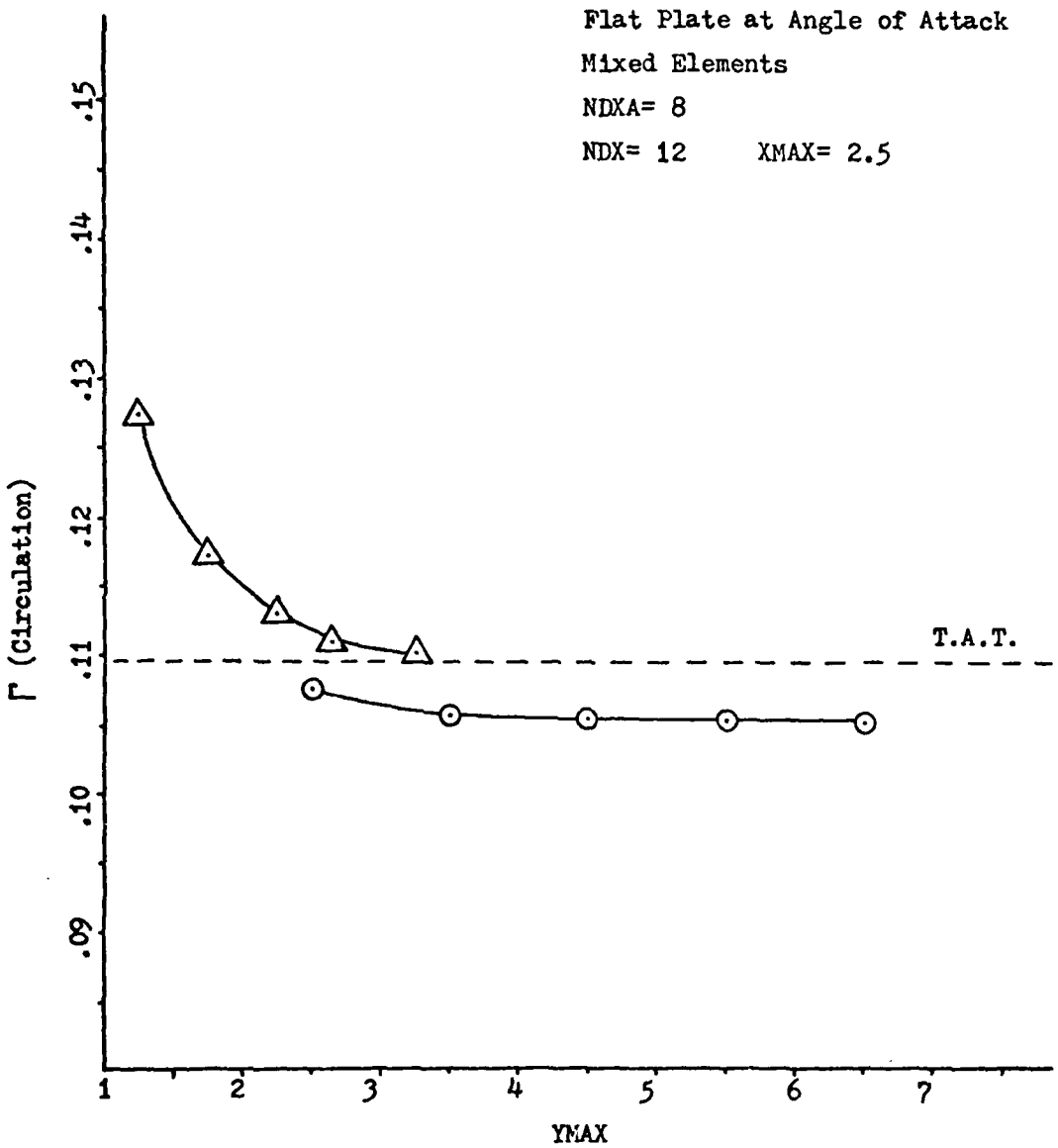

Symbol	AR
△	1.00
⊙	0.50

Figure 20. Mixed Elements, Constant Aspect Ratio, Expansion of Domain in y-direction

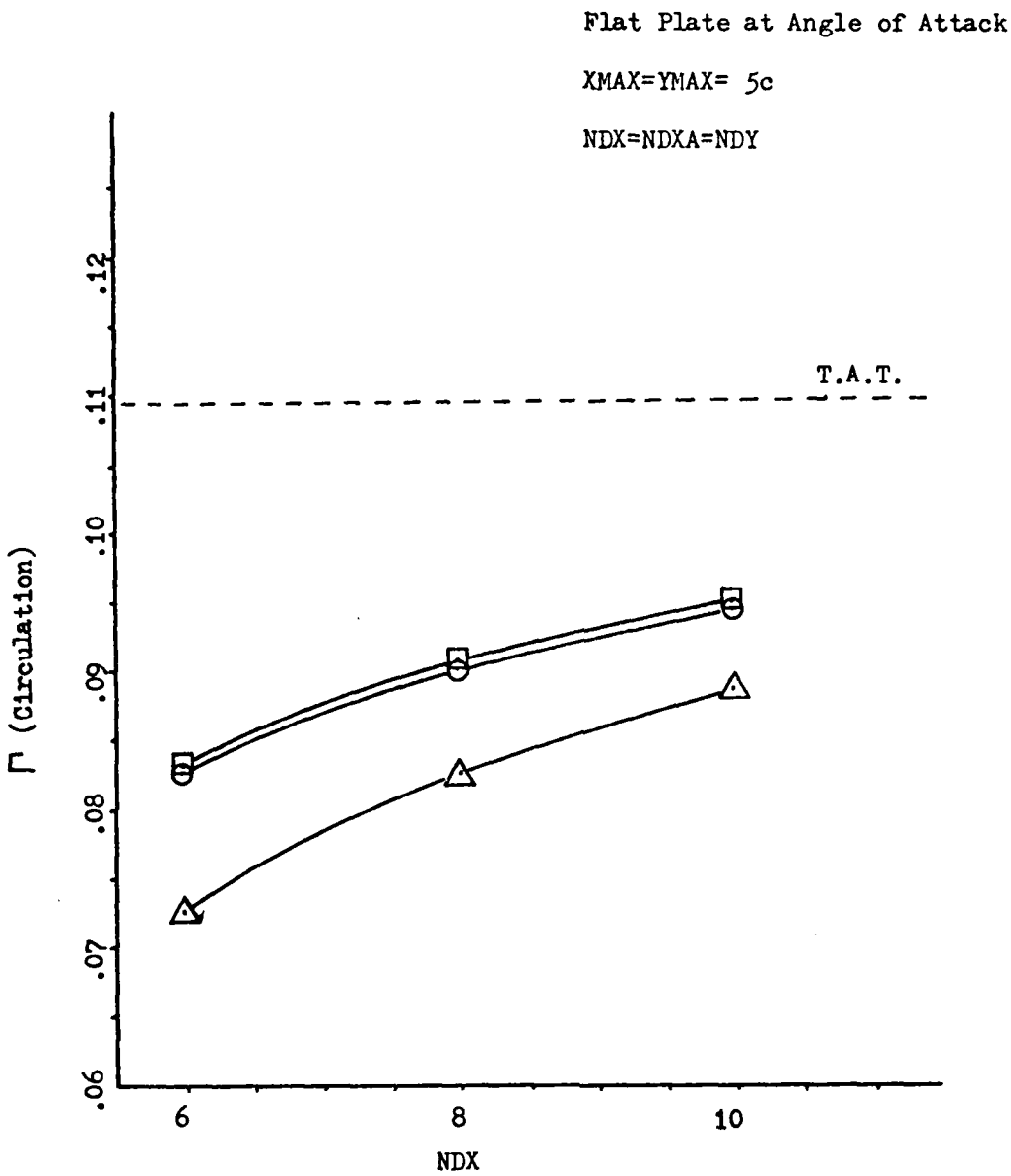

Symbol	Grid
△	Linear Elements - Uniformly Spaced
⊙	Linear Elements - with small TE element
⊡	Mixed Elements

Figure 21. Convergence of Circulation of Mixed Elements Compared to Linear Equally Spaced Grids

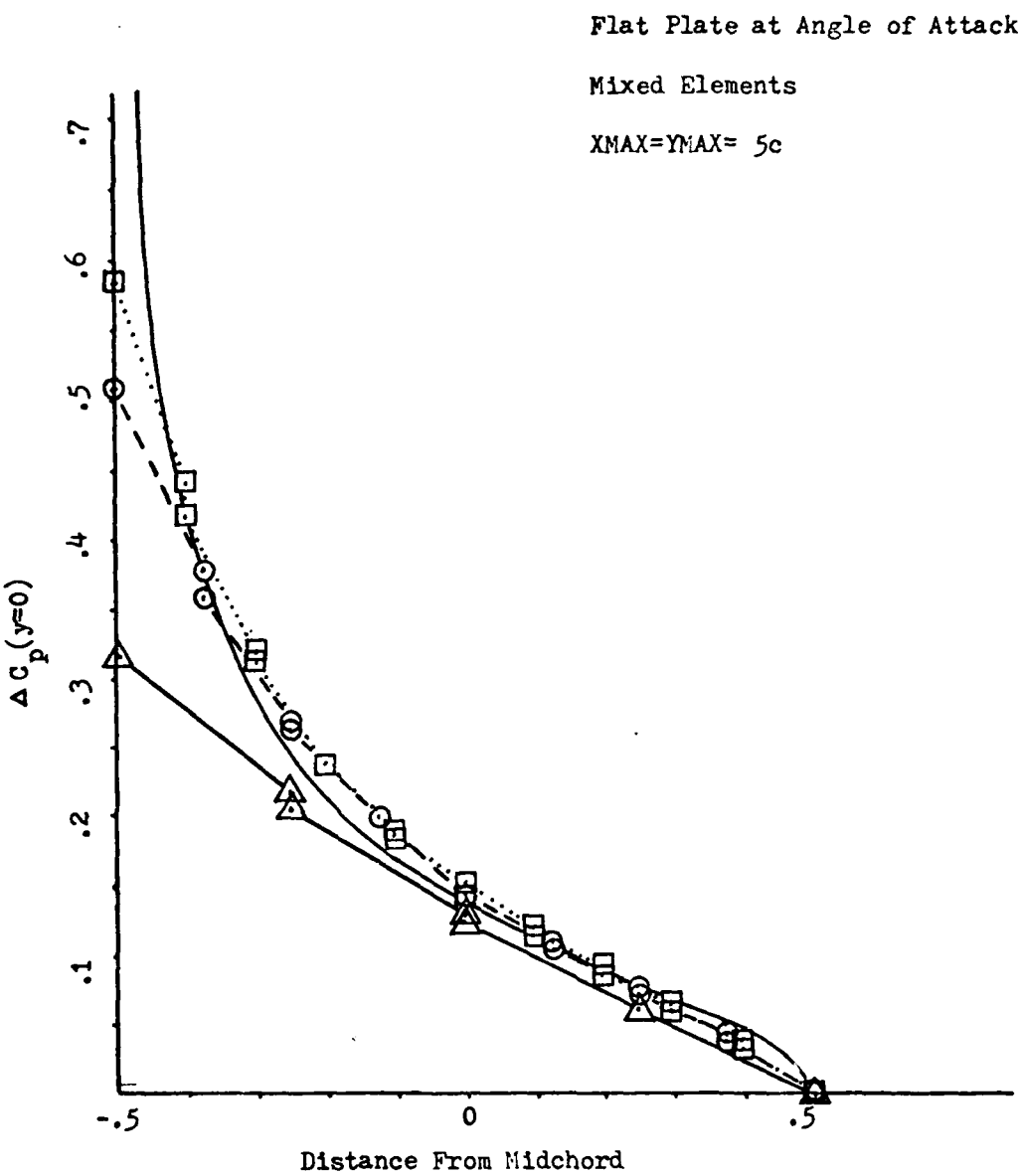

Symbol	Nodes	Elements	NDX	NDXA	NDY
△	59	32	4	4	4
⊙	181	128	8	8	8
⊡	266	200	10	10	10

Figure 22. Pressure Distribution For Mixed Elements and Uniform Reduction of Element Size

linear elements with small trailing edge element in Fig 10, the reason for virtually the same circulation with similar parameters becomes apparent. The value of the pressure coefficient in each comparable element at the midpoint of the element is virtually the same in each case. The advantage to the mixed elements; however, is the improved approximation compared to the exact curve that is obtained with the linear distribution within the element. Another characteristic of the mixed element is the jump in pressure at the interface of each element. This jump is very small except at and near the leading edge. The cause of this jump, is due to the large change in the slope of the exact solution near the leading edge. In attempting to approximate this change, the elemental slopes are also changing by large amounts in this region. This causes the potentials at the common nodes to vary. The conclusions of the previous section concerning the convergence of the pressure distribution to the exact value from thin-airfoil theory apply in this case, with the mixed elements producing a better approximation to the exact distribution.

Quadratic Elements

The third type of element used was a quadratic, Lagrange, element which was used throughout the flowfield, Fig 23. The elemental equation formulation is demonstrated in Appendix B. As in the mixed elements on the airfoil, the quadratic elements allow the Kutta condition to be applied at the last node on the airfoil. The u velocity and pressure are also linear along the airfoil boundary.

Farfield Boundary Location.

The same procedures used for determining the farfield boundary location for the linear elements were also used for the quadratic

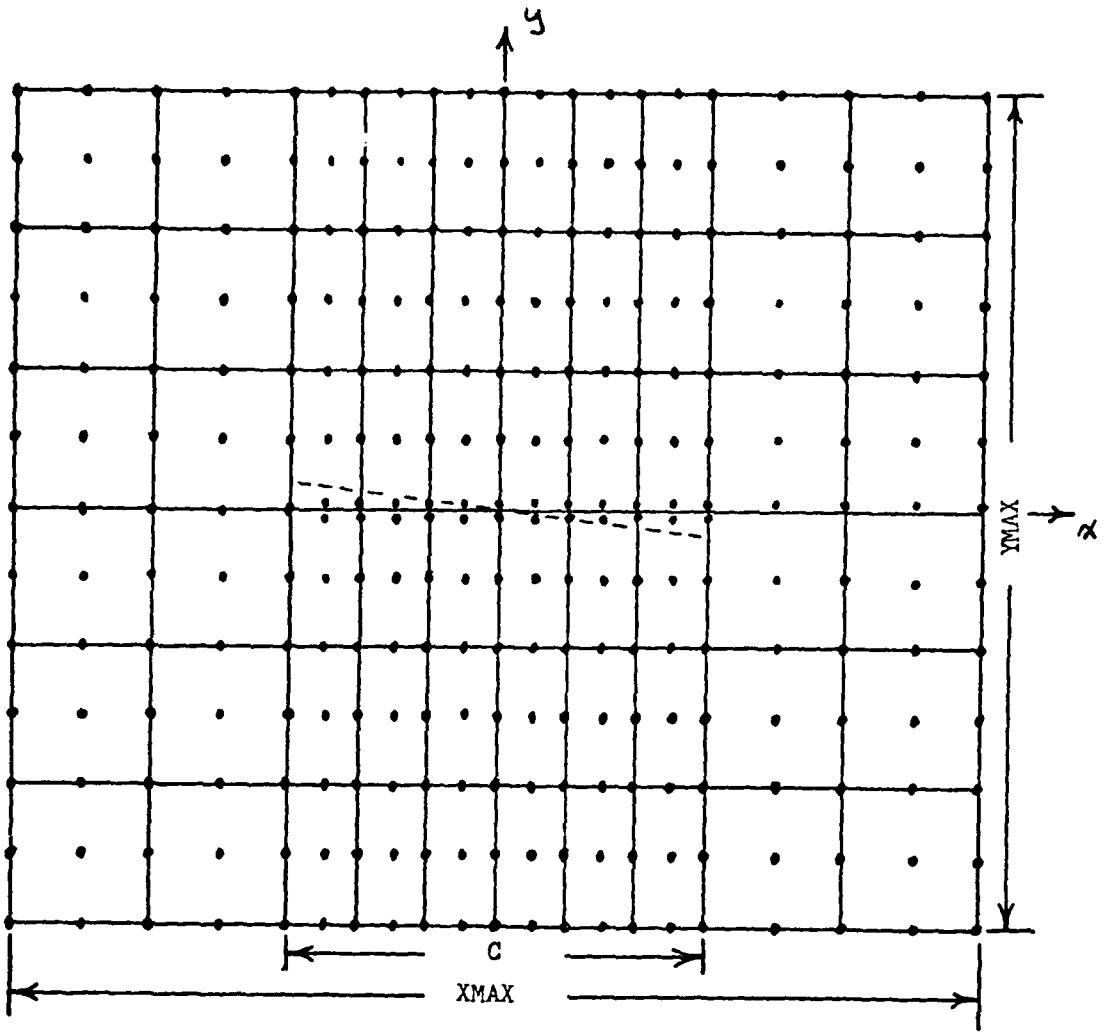

Figure 23. Quadratic Element Discretization

elements. The results of expanding the field in the x-direction are shown in Fig 24, while the results for the subsequent expansion in the y-direction is shown in Fig 25. In this case a farfield boundary location greater than XMAX= 3.5c and YMAX= 3.5c has no effect on the pressure distribution on the airfoil.

Pressure Coefficient.

The effect of element size on the pressure distribution is accomplished as was done for the linear elements. The result for uniform reduction of the element size parameters is shown in Fig 26. This figure shows that element refinement produces very fast convergence from the quarter chord to the trailing edge. Near the leading edge convergence is much slower, as the slope of the approximation is changing very fast in this region. In general it can be said that even a coarse mesh produces a reasonable approximation to the exact thin-airfoil theory value. As elements are refined it is evident that the error in the pressure becomes smaller. This fact is also reflected in the improvement of circulation. The trend of the solution is seen to approach the exact as element size is reduced, which is the desireable trend.

The results for reduction of the farfield size parameters only are shown in Fig 27. In this coarse grid, only four elements on the airfoil, there is little change in the pressure distribution from the quarter-chord to the trailing edge. Keeping the airfoil elements constant and reducing the farfield elements produces a significant jump at the interface of the first two elements. This jump increases with decreasing size of the farfield elements. This can be attributed again to the slope in the first two elements, as occurred in the mixed elements.

The results for the reduction of the element width over the airfoil

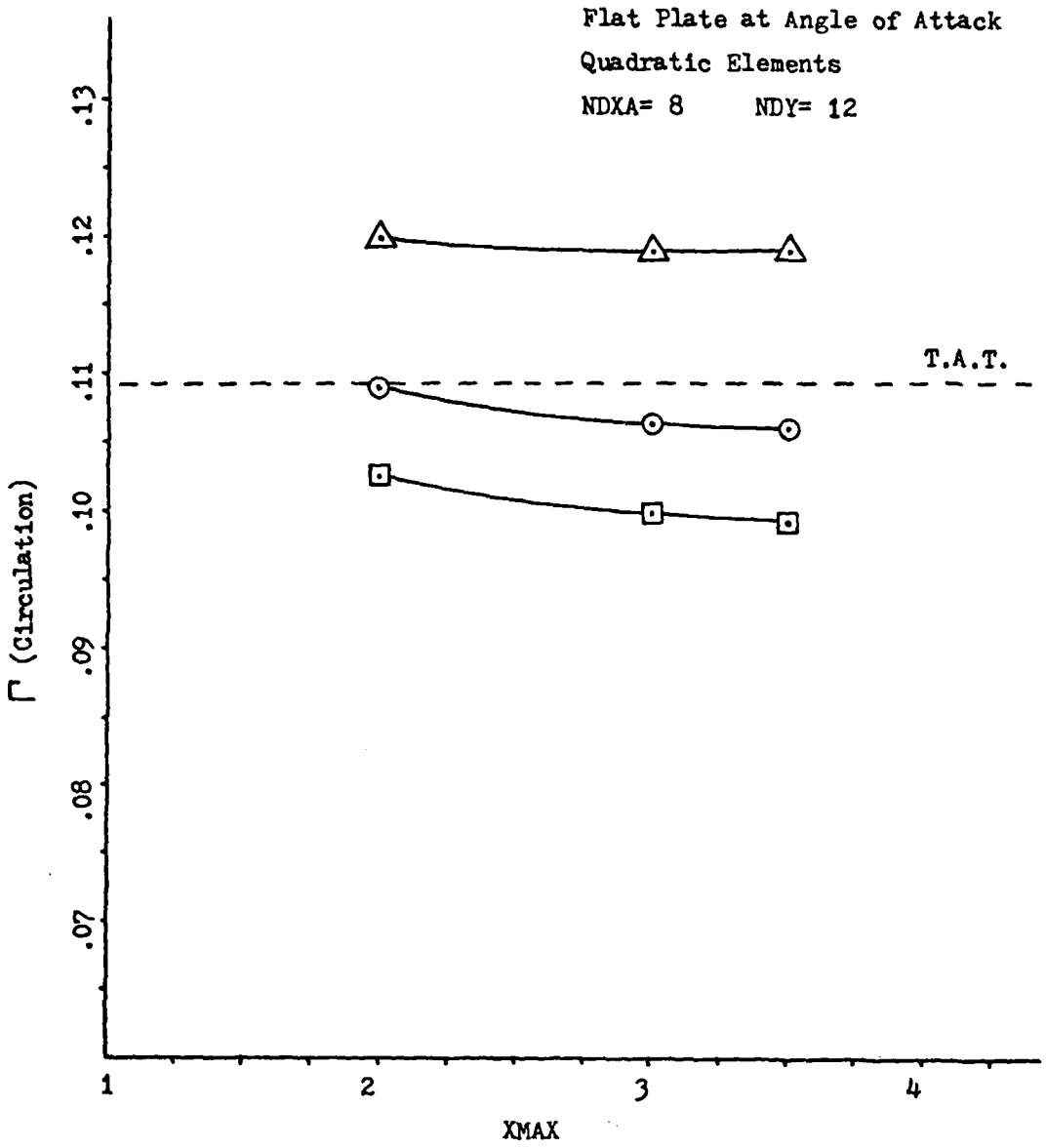

Symbol	AR	YMAX
△	1.00	1.5
⊙	0.50	3.0
⊡	0.25	6.0

Figure 24. Quadratic Elements, Constant Aspect Ratio, Expansion of Domain in x-direction

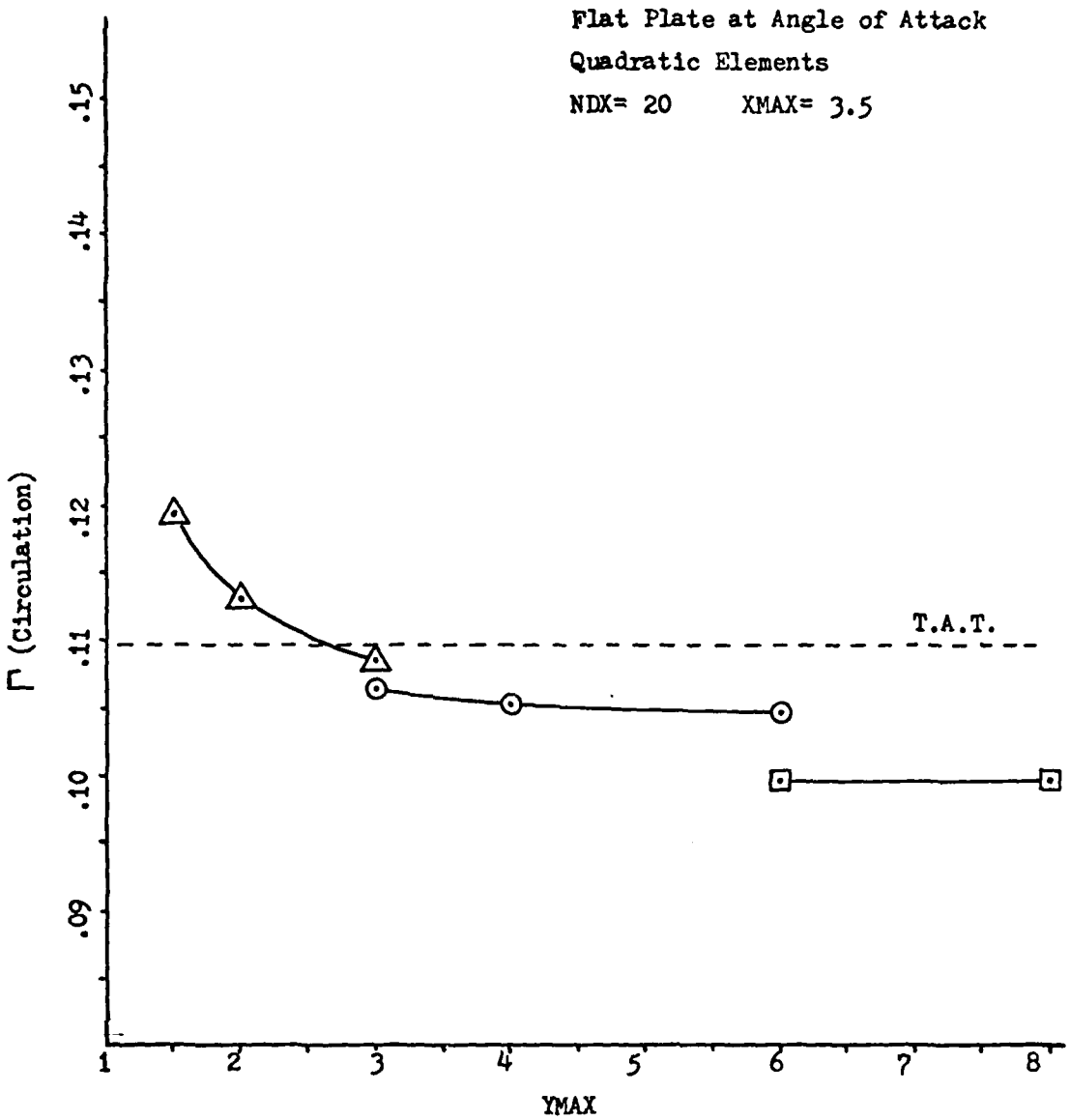

Symbol	AR
△	1.00
⊙	0.50
⊡	0.25

Figure 25. Quadratic Elements, Constant Aspect Ratio, Expansion of Domain in y-direction

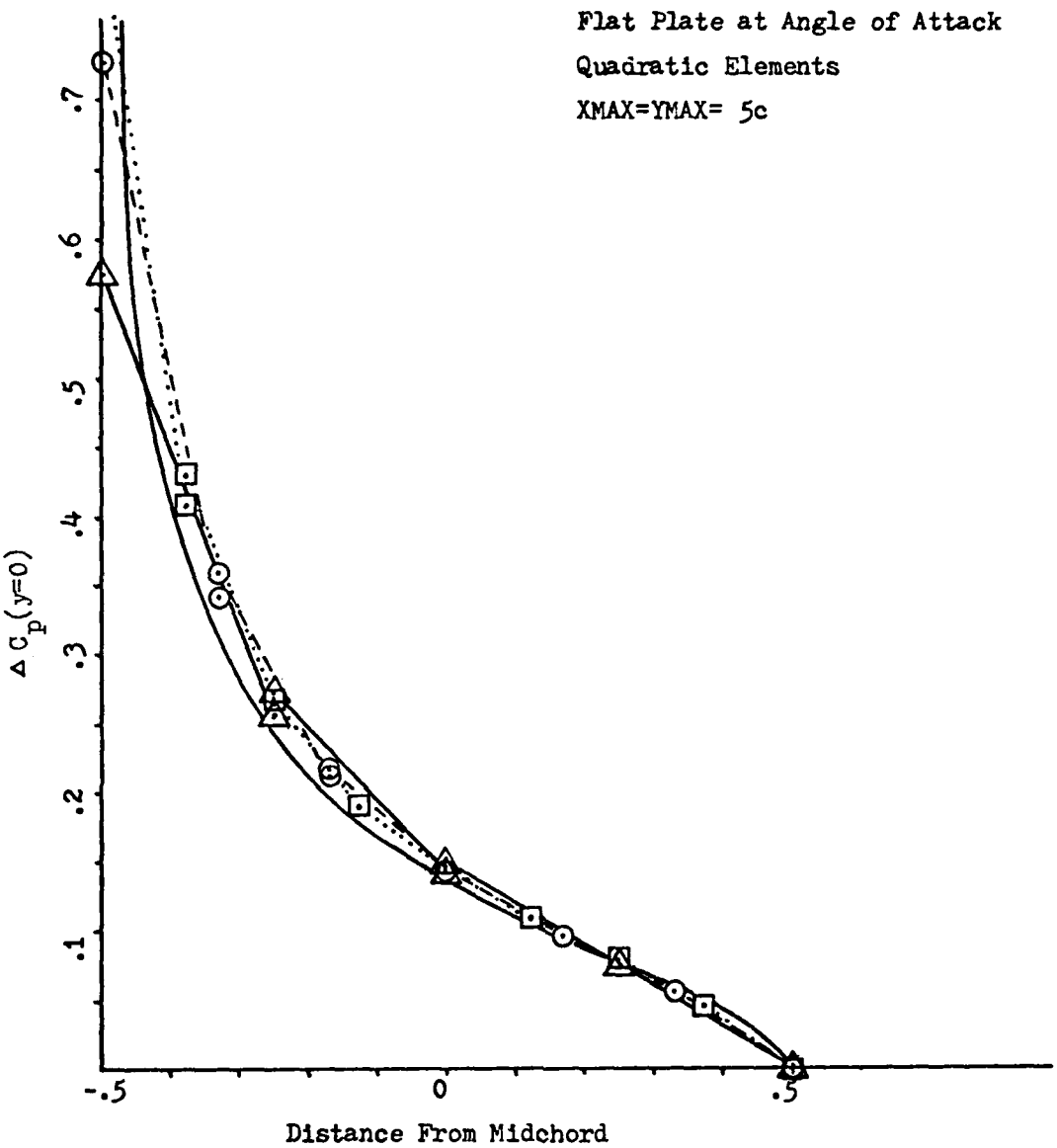

Symbol	Nodes	Elements	NDX	NDXA	NDY
△	165	32	8	8	8
⊙	343	72	12	12	12
⊡	585	128	16	16	16

Figure 26. Pressure Distribution For Quadratic Elements and Uniform Reduction of Element Size

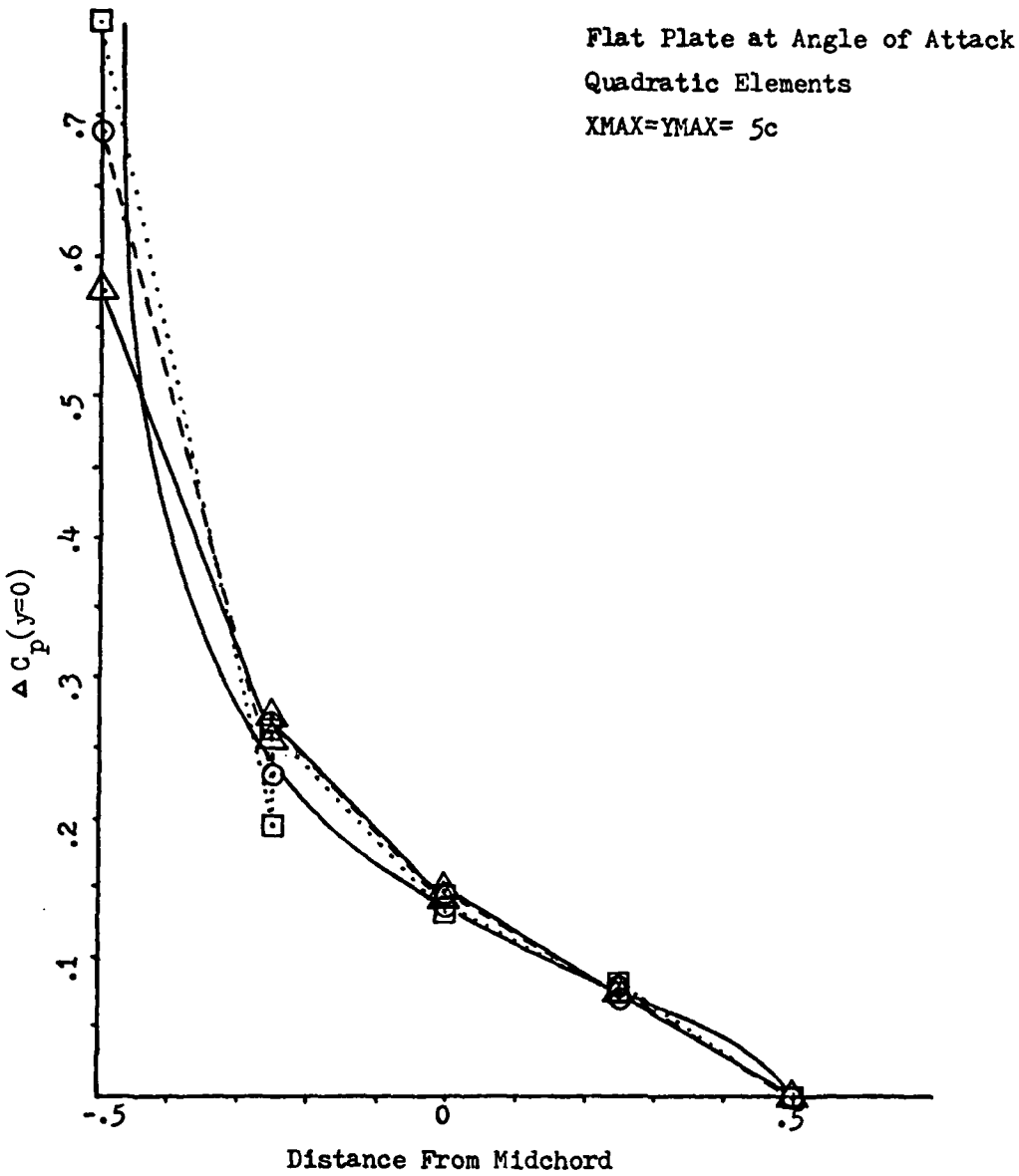

Symbol	Nodes	Elements	NDX	NDXA	NDY
△	165	32	8	8	8
⊙	287	60	12	8	12
⊡	441	96	16	8	16

Figure 27. Pressure Distribution For Quadratic Elements and Uniform Reduction of Farfield Parameters Only

only is shown in Fig 28. The results show that refinement in this manner does not significantly improve the leading edge approximation, but does on the average improve the approximation at each point to the exact.

From these observations, the same conclusions concerning discretization that were made for linear elements apply to the quadratic elements. A comparison of the pressure distributions obtained with linear elements, mixed elements, and quadratic elements with the element size parameters the same is shown in Fig 29. It is evident from this figure that the improvement in circulation is due to a closer approximation at the leading edge for the quadratic element. It is also seen that when using the midpoint of the linear elements for comparison, there is little difference in the three elements from the quarterchord to the trailing edge.

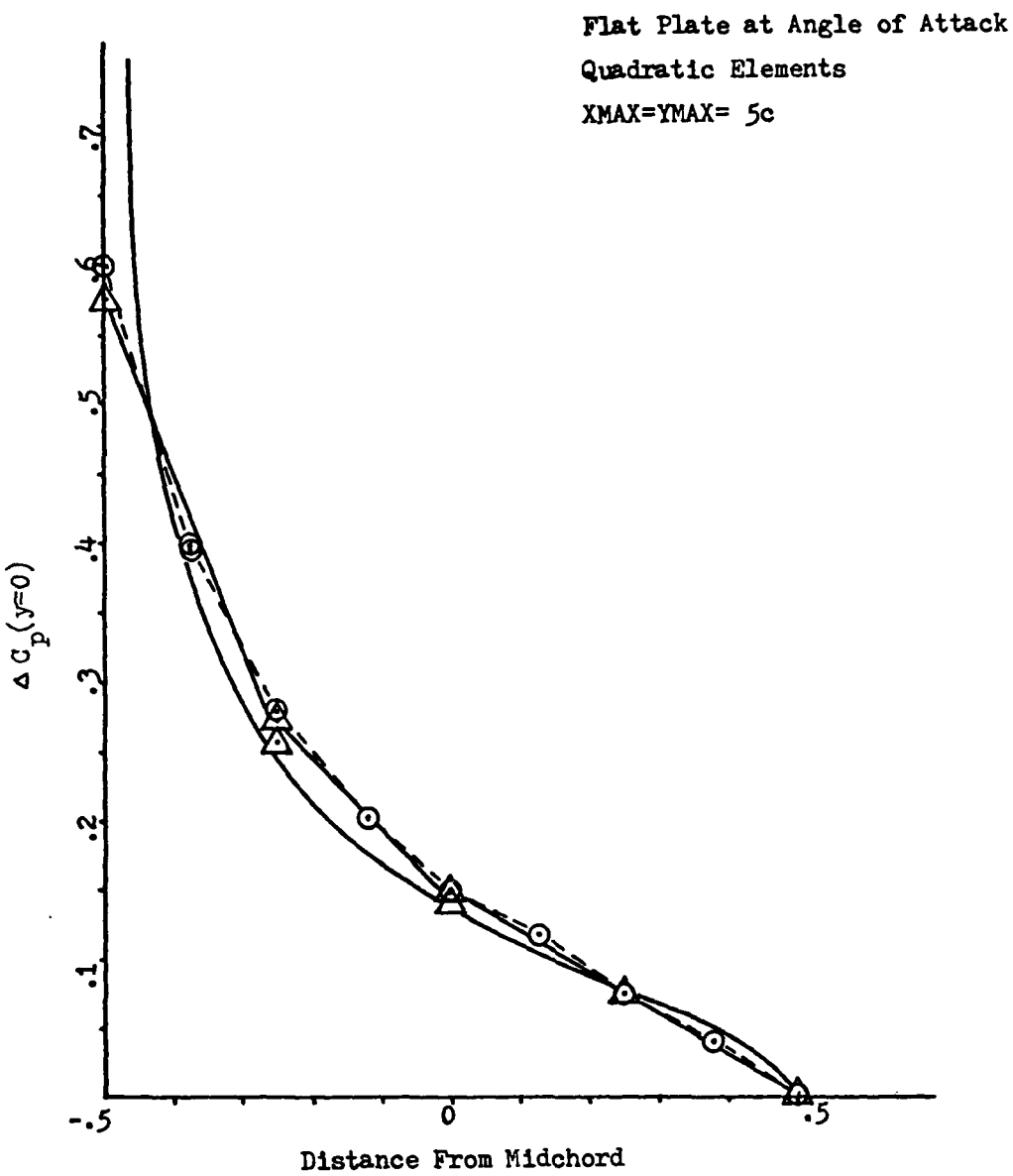

Symbol	Nodes	Elements	NDX	NDXA	NDY
△	165	32	8	8	8
⊙	245	48	8	16	8

Figure 28. Pressure Distribution For Quadratic Elements And Reduction of Airfoil Element Width Parameter Only

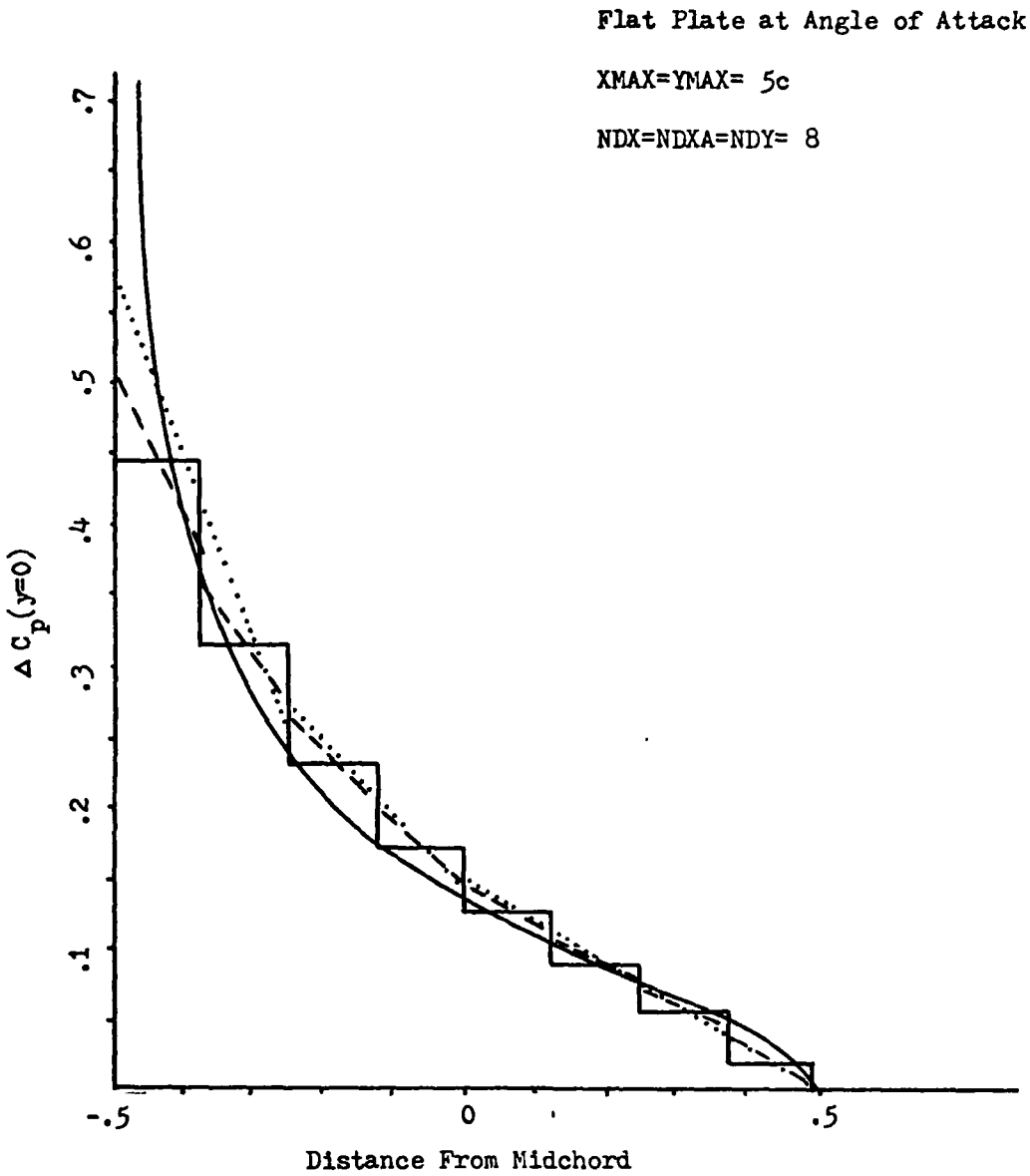

Line	Nodes	Elements	Γ	Type Element
———	175	136	.0902	Linear w TE Element
– – –	181	128	.0904	Mixed Element
·····	165	32	.0961	Quadratic Element

Γ (exact)= .1097

Figure 29. Pressure Distribution Comparison of Linear, Mixed, and Quadratic Elements

V Conclusions and Recommendations

The Galerkin Finite Element Method was shown to be an effective means of approximating the solution to the steady, two-dimensional, incompressible, potential flow over a thin lifting airfoil. Three types of elements were used over the airfoil to investigate the farfield boundary location and the pressure distribution over the airfoil.

The Superposition Method of solution was seen to be the best of the three solution methods used from the standpoint of computer storage and computation time. It was found through comparison of the results of this method with those of Iterative Method 2, that the constraint of the x-velocity being zero along the branch cut has negligible influence on the pressure distribution and circulation.

The infinite domain of the problem was approximated by a finite domain. It was desireable to make this domain as small as possible without affecting the results. This was accomplished by expansion of a base solution of constant aspect ratio elements in first the x-direction and then the y-direction. The result of this procedure showed that the infinite domain could be approximated by a relatively small finite domain. The domain of the linear elements could be approximated by XMAX=2.5c and YMAX=3.0c. The domain of the mixed elements could be approximated by XMAX=2.5c and YMAX=3.0c, while the quadratic element domain was XMAX=3.5c and YMAX=3.5c. Although the quadratic element domain is slightly larger, the number of elements used is much smaller, 14 in both the x- and y-directions versus 20 and 24 in the x- and y-directions respectively for the linear elements.

The use of linear elements throughout the flowfield and on the

surface of the airfoil was investigated for three grid patterns. It was seen that using a uniform grid over the domain was not an efficient method, due to the singularity at the leading edge and the application of the Kutta condition at the trailing edge, which effectively made the airfoil smaller. A correction to this grid was made by adding a small element at the trailing edge. This modification made a significant improvement in the convergence of the pressure distribution to the exact, by eliminating the loss of pressure at the trailing edge with coarse grids. A third grid that varied the size of elements, concentrating small elements at the leading and trailing edges, produced the fastest convergence to the exact circulation value. This was due to the improvement in the approximation at the leading edge singularity.

The use of mixed (transition) elements on the airfoil surface with linear elements everywhere else was next investigated. This element was an improvement over the linear element in approximating the pressure distribution. This was due to the linear variation in the mixed element as opposed to the step function distribution of the linear element. This element also eliminated the problem of applying the Kutta condition as was experienced at the trailing edge with the linear elements. Although this element produces an improved pressure distribution over the linear elements, the circulation is effectively the same.

The use of quadratic, Lagrange, elements over the airfoil surface and in the farfield improved the convergence of the circulation to the exact, when compared to uniformly spaced linear and mixed elements, with an equivalent number of nodes. Some care must be exercized when using a coarse grid over the airfoil due to the jump in pressure at the element boundaries, near the leading edge. A major disadvantage of this element

is the large number of degrees-of-freedom associated with it.

From the above considerations, it can be concluded that a variable geometry grid with small elements concentrated at the leading and trailing edges provides the best results for the approximation of the circulation. This is further evidenced by comparing the quadratic element results with the linear elements at an equal number of degrees-of-freedom. For 165 nodes the circulation value for the quadratic elements is 12.4% below the thin-airfoil theory value, while the linear exponentially spaced grid is only 4.2% below thin-airfoil theory.

The pressure distribution is best approximated by a quadratic interpolation, the mixed or quadratic elements, on the airfoil surface. The combination of the mixed elements on the airfoil surface and linear elements in the farfield provides a reasonable approximation to the exact thin-airfoil theory, without the disadvantage of the extra degrees-of-freedom required by the quadratic elements.

Recommendations For Future Work

This investigation should serve as a basis for further work in the application of the Finite Element Method to the thin-airfoil problem. Extension of the method to the cambered and thickness portions of the airfoil problem are necessary. An analysis of this problem for the convergence of the circulation and pressure distribution as was accomplished for the flat-plate at angle of attack should be done. The treatment of the branch cut when the method is applied to the thickness problem needs to be addressed. In this case the circulation is zero and the x-direction velocity in the branch cut cannot be zero.

The treatment of the farfield boundary requires further investigation. In this report no potential values were defined on the farfield

boundary. A method for defining the potentials on the farfield boundary would reduce the system of equations to be solved through partitioning.

Further investigation of grid refinement needs to be made. The concentration of small elements at the leading and trailing edges should be extended to include the mixed and quadratic elements. The effect of placing a mid-side node, from either the mixed or quadratic element, at the leading and trailing edges should be reviewed.

Other types of elements, such as Hermitian, to guarantee continuity of the pressure at element boundaries, infinite elements, that do not require the finite boundary, or special elements to improve the approximation at the leading edge singularity could also be applied to this problem.

The orientation of the branch cut in this report was restricted to extension horizontally from the trailing edge to the farfield boundary along $y=0$. The effect of changing this orientation, such as approximating it with a function whose slope at the trailing edge were equal to the angle of attack and that became horizontal at some distance behind the trailing edge, should be compared with the results obtained here.

Bibliography

1. Huebner, Kenneth H. The Finite Element Method For Engineers. New York: John Wiley & Sons, 1975.

2. Norris, D.H. and G. de Vries. An Introduction To Finite Element Analysis. New York: Academic Press, 1978.

3. Chung, T.J. Finite Element Analysis In Fluid Dynamics.New York: McGraw-Hill International Book Company, 1978.

4. Zienkiewicz, O. and Y.K. Cheung. "Finite Elements in the Solution of Field Problems", The Engineer (Sept 1965).

5. Martin, H.C. "Finite Element Analysis of Fluid Flow", AFFDL-TR-68-150, Proceedings of the Second Conference On Matrix Methods in Structural Mechanics, Wright-Patterson AFB, Ohio:(Dec 69).

6. de Vries, G. and D.H. Norrie. The Application Of The Finite Element Technique To Potential Flow Problems: Part I. University of Calgary: Mechanical Engineering Department Report No. 7. (August 1969).

7. de Vries, G. and D.H. Norrie. The Application Of The Finite Element Technique To Potential Flow Problems: Part II. University of Calgary: Mechanical Engineering Department Report No. 8 (July 1969).

8. de Vries, G. and D.H. Norrie. "Application of the Finite Element Technique to Potential Flow Problems", Journal Of Applied Mechanics: 798-802 (December 1971).

9. Cary, G.F. "A Dual Perturbation Expansion and Variational Solution For Compressible Flows Using Finite Elements". Finite Elements In Fluids Vol II. New York: John Wiley, 1975.

10. Shen, S.F. "An Aerodynamicist Looks at the Finite Element Method", Finite Elements in Fluids Vol II. New York: John Wiley, 1975.

11. Habashi, Wagdi G. "The Finite Element Method In The Solution Of Unbounded Potential Flows", International Journal For Numerical Methods in Engineering, Vol 14, 1347-1358, (1979).

12. Baskharone, E. and A. Hamed. "A New Approach In Cascade Flow Analysis Using The Finite Element Method", AIAA Journal, Vol 19, No 1 (Jan 81).

13. Shapiro, Ascher H. The Dynamics And Thermodynamics Of Compressible Fluid Flow. New York: John Wiley & Sons, 1953.

14. Karamcheti, Krishnamurty. Principles of Ideal-Fluid Aerodynamics. Malabar: Robert E. Krieger Publishing Company, 1980 (Revision).

15. Marsh, James E. Prediction of Aerodynamic Forces on a Circular Cylinder And a Thin Airfoil In a Transonic Airstream By The Finite Element Method. AFIT/DS/AA/79M-1. Wright-Patterson AFB, Ohio: Air Force Institute of Technology, 1979.

Appendix A

Finite Element Equations For Flow Over an Airfoil For a Bilinear, Rectangular Element

Interpolation Functions

The interpolation functions for the bilinear rectangular element shown in Fig 30 are given by

$$N_1(\xi,\eta) = \tfrac{1}{4}(\xi+1)(\eta+1) \tag{A-1}$$

$$N_2(\xi,\eta) = \tfrac{1}{4}(\xi-1)(\eta+1) \tag{A-2}$$

$$N_3(\xi,\eta) = \tfrac{1}{4}(\xi-1)(\eta-1) \tag{A-3}$$

$$N_4(\xi,\eta) = \tfrac{1}{4}(\xi+1)(\eta-1) \tag{A-4}$$

$$\xi = (x-x_c)/a \qquad \eta = (y-y_c)/b$$

Coordinates (ξ,η) are the local nodal coordinates.

Elemental Equations

The Finite element equations obtained from the governing differential equation and written in elemental form are expressed by equation (31) as

$$A_{ij}\,\phi_j = f_i \tag{A-5}$$

where

$$A_{ij} = \iint_{\Omega_e}\left(\frac{\partial N_j}{\partial x}\frac{\partial N_i}{\partial x} + \frac{\partial N_j}{\partial y}\frac{\partial N_i}{\partial y}\right)dx\,dy \tag{A-6}$$

$$f_i = \int_{\partial\Omega^*} \frac{df}{dx} N_i \Big|_{y=0} dx \tag{A-7}$$

Global coordinates (x,y) are transformed to the local coordinates

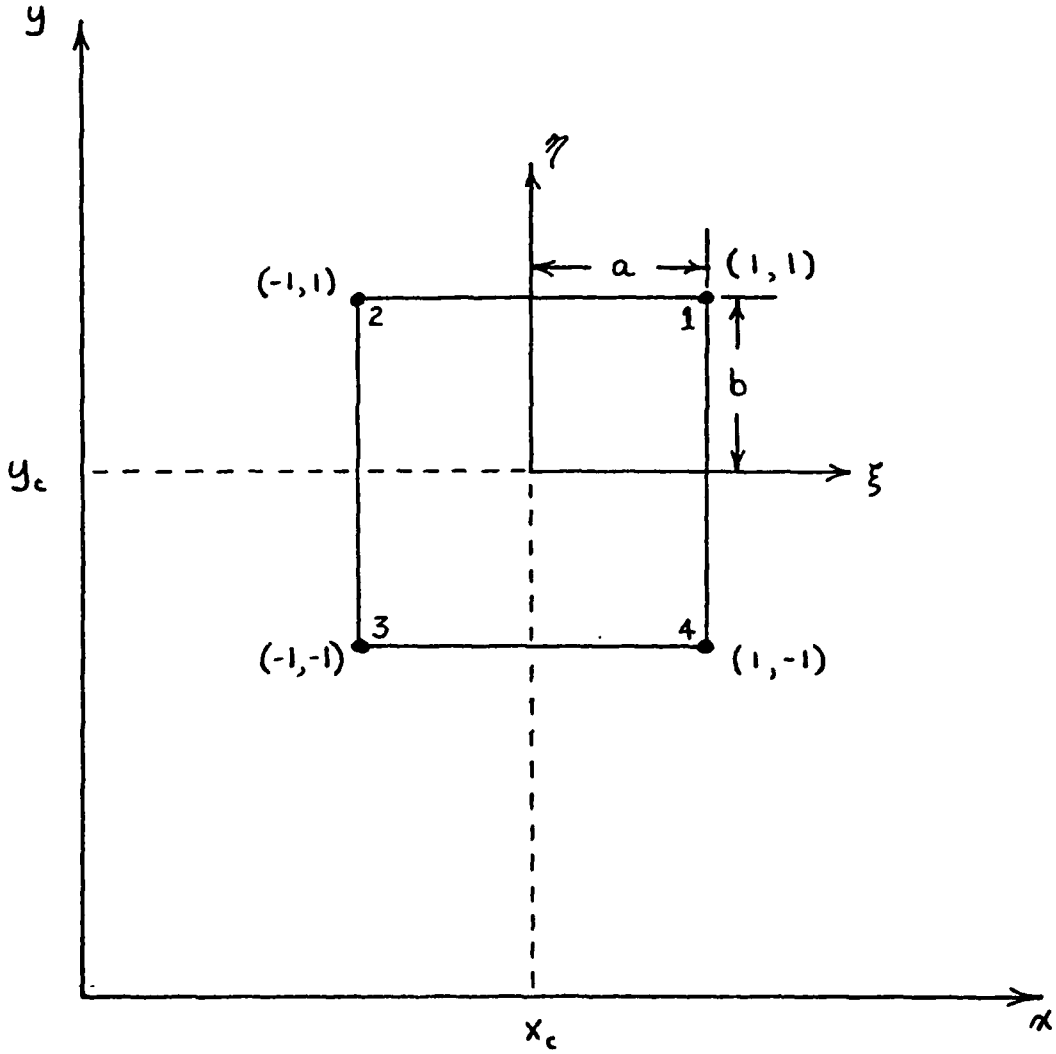

Figure 30. Bilinear Rectangular Element

(ξ, η) by the transformation equations:

$$\xi = \frac{x - x_c}{a} \qquad \eta = \frac{y - y_c}{b}$$

$$\frac{\partial N_j}{\partial x} = \frac{1}{a}\frac{\partial N_j}{\partial \xi} \qquad \frac{\partial N_j}{\partial y} = \frac{1}{b}\frac{\partial N_j}{\partial \eta} \tag{A-8}$$

$$dx = a\, d\xi \qquad dy = b\, d\eta$$

From these expressions, the elemental equations can be written in the form

$$A_{ij} = \int_{-1}^{+1}\int_{-1}^{+1} \left(\frac{b}{a}\frac{\partial N_j}{\partial \xi}\frac{\partial N_i}{\partial \xi} + \frac{a}{b}\frac{\partial N_j}{\partial \eta}\frac{\partial N_i}{\partial \eta} \right) d\xi\, d\eta \tag{A-9}$$

$$f_i = a \int_{-1(+1)}^{+1(-1)} \frac{df}{dx}(\xi)\, N_i \Big|_{\eta = \pm 1} d\xi \tag{A-10}$$

The matrix A_{ij} is dependent only on the size of the element and not directly on any particular airfoil contour. Substituting the interpolation functions, A-1 through A-4, into A-5 results in

$$A_{ij} = \begin{bmatrix} A+B & -A+\frac{B}{2} & -\frac{(A+B)}{2} & \frac{A}{2}-B \\ & A+B & \frac{A}{2}-B & -\frac{(A+B)}{2} \\ & & A+B & -A+\frac{B}{2} \\ (SYM) & & & A+B \end{bmatrix} \tag{A-11}$$

where $A = \dfrac{b}{3a}$ and $B = \dfrac{a}{3b}$

The vector f_i is directly dependent on the airfoil surface contour. This quantity is evaluated only for elements that share a common boundary with the surface. For all other elements, this vector is zero.

Velocity Distribution

The velocity in element e is calculated from the assumed solution for the potential given by eq 24

$$\phi^e(x,y) = N_j(x,y)\,\phi_j^{\,e} \tag{24}$$

From the definition of the potential function

$$u = \frac{\partial\phi}{\partial x} \qquad v = \frac{\partial\phi}{\partial y} \tag{A-12}$$

and through transformation to local coordinates (ξ,η)

$$u = \sum_{j=1}^{4} \frac{1}{a}\frac{\partial N_j}{\partial\xi}(\xi,\eta)\,\phi_j \tag{A-13}$$

$$v = \sum_{j=1}^{4} \frac{1}{b}\frac{\partial N_j}{\partial\eta}(\xi,\eta)\,\phi_j \tag{A-14}$$

The x-direction velocity on the top surface, $\eta=-1$, u becomes

$$u_u = \frac{\phi_4 - \phi_3}{2a} \tag{A-15}$$

Likewise on the lower surface, $\eta=+1$, u becomes

$$u_L = \frac{\phi_1 - \phi_2}{2a} \tag{A-16}$$

Pressure Distribution

For steady, small-disturbance theory the coefficient of pressure is given by (Ref 13)

$$C_p = -2u \tag{A-17}$$

From thin-airfoil theory, the pressure coefficient is evaluated along $y=0^{\pm}$. Thus for element e which borders the airfoil surface, the elemental pressure coefficient becomes

$$C_p^e(x, y=0^{\pm}) = \sum_{j=1}^{4} -\frac{2}{a}\frac{\partial N_j}{\partial \xi}(\xi, \eta=\pm 1)\,\phi_j^e \tag{A-18}$$

For an upper surface element, $\eta=-1$, C_p becomes

$$C_{P_U}^e = -\frac{1}{a}(\phi_4 - \phi_3) \tag{A-19}$$

For a lower surface element, $\eta=+1$, C_p becomes

$$C_{P_L}^e = -\frac{1}{a}(\phi_1 - \phi_2) \tag{A-20}$$

Within the element e, the pressure is a constant value, which results in "jumps" in pressure between elements along the airfoil surface. The pressure distribution along $y=0^{\pm}$ is; therefore, a step function for the bilinear rectangular element.

Boundary Influence

Those elements along the airfoil surface will produce non-zero forcing terms f_i. The forcing term is determined by evaluating eq A-7

for each element

$$f_i^e = \int_{\partial\Omega} \frac{df}{dx} N_i \Big|_{y=0} dx \tag{A-21}$$

For a flat plate at angle of attack α , $\frac{df}{dx} = -\alpha$ .Converting the integral to the local coordinate system gives

$$f_i^e = \int_{\partial\Omega} -\alpha a N_i \Big|_{y=0} d\xi \tag{A-22}$$

For elements along the lower surface the forcing terms are determined from

$$f_i = -\alpha a \int_{-1}^{+1} N_i(\xi, \eta = +1)\, d\xi \tag{A-23}$$

For elements along the upper surface the forcing terms are determined from

$$f_i = -\alpha a \int_{+1}^{-1} N_i(\xi, \eta = -1)\, d\xi \tag{A-24}$$

Appendix B

Finite Element Equations For Flow Over an Airfoil For a Biquadratic, Lagrange, Rectangular Element

Interpolation Functions

The interpolation functions for the biquadratic, Lagrange, rectangular element shown in Fig 31 are given by (Ref 3)

$$N_1 = \frac{\xi}{2}(\xi - 1)\frac{\eta}{2}(\eta - 1) \tag{B-1}$$

$$N_2 = \frac{\xi}{2}(\xi + 1)\frac{\eta}{2}(\eta - 1) \tag{B-2}$$

$$N_3 = \frac{\xi}{2}(\xi + 1)\frac{\eta}{2}(\eta + 1) \tag{B-3}$$

$$N_4 = \frac{\xi}{2}(\xi - 1)\frac{\eta}{2}(\eta + 1) \tag{B-4}$$

$$N_5 = (1 - \xi^2)\frac{\eta}{2}(\eta - 1) \tag{B-5}$$

$$N_6 = \frac{\xi}{2}(\xi + 1)(1 - \eta^2) \tag{B-6}$$

$$N_7 = (1 - \xi^2)\frac{\eta}{2}(\eta + 1) \tag{B-7}$$

$$N_8 = \frac{\xi}{2}(\xi - 1)(1 - \eta^2) \tag{B-8}$$

$$N_9 = (1 - \xi^2)(1 - \eta^2) \tag{B-9}$$

where $$\xi = \frac{(x - x_c)}{a} \qquad \eta = \frac{(y - y_c)}{b} \tag{B-10}$$

Coordinates (ξ, η) are the local nodal coordinates.

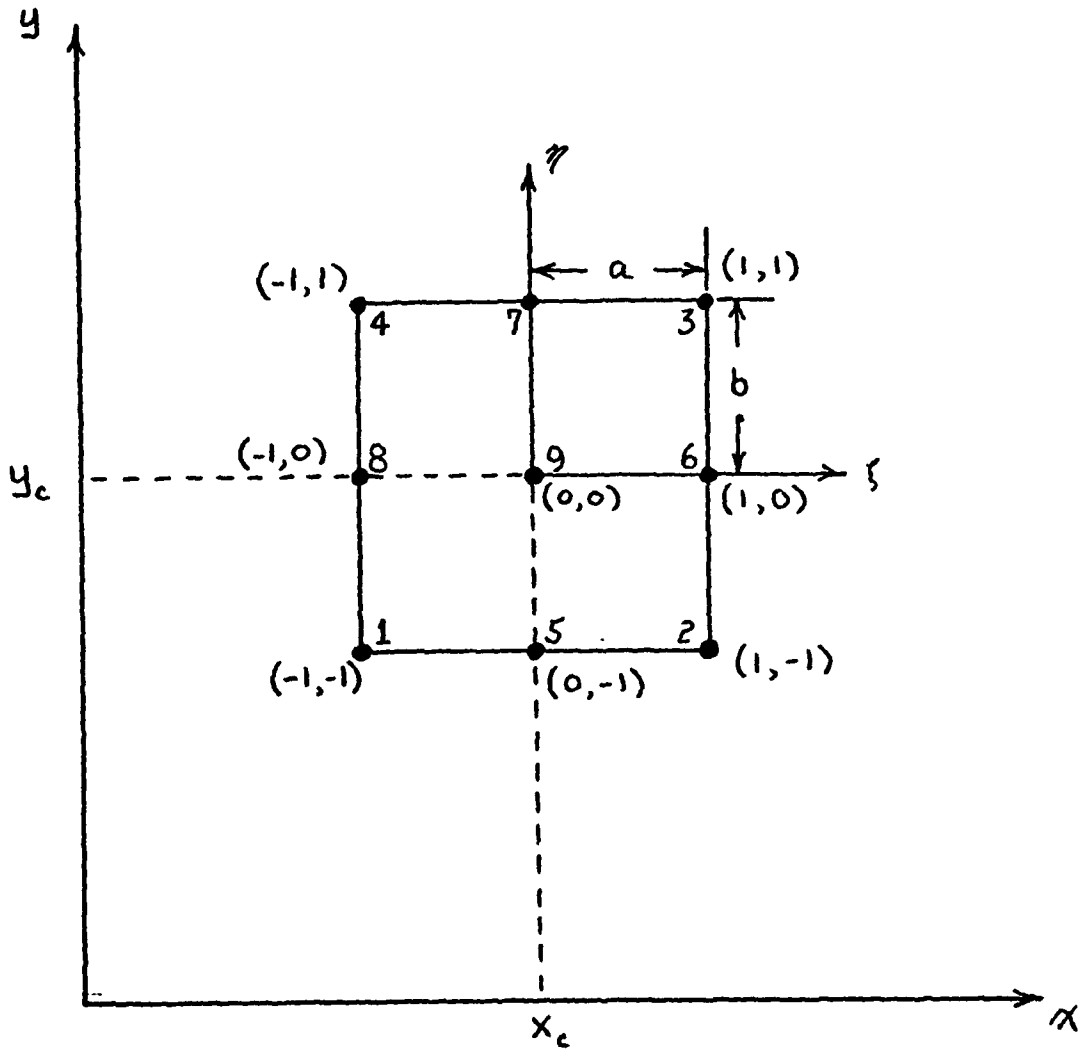

Figure 31. Biquadratic, Lagrange, Element

Elemental Equations

The elemental equations are the same as those derived for the bilinear rectangular element, eq A-5 through A-7,

$$A_{ij}\phi_j = f_i \tag{A-5}$$

$$A_{ij} = \int_{-1}^{+1}\int_{-1}^{+1}\left(\frac{b}{a}\frac{\partial N_j}{\partial \xi}\frac{\partial N_i}{\partial \xi} + \frac{a}{b}\frac{\partial N_j}{\partial \eta}\frac{\partial N_i}{\partial \eta}\right)d\xi\, d\eta \tag{A-6}$$

$$f_i = a\int_{-1(+1)}^{+1(-1)} \frac{df}{dx}(\xi)N_i\Big|_{\eta=\pm 1} d\xi \tag{A-7}$$

The first matrix A_{ij} is only dependent on the size of the element and not directly on any particular airfoil contour. Substituting the interpolation functions, B-1 through B-9, into A-5 results in the matrix shown in Fig 32.

The vector f_i is directly dependent on the airfoil surface contour. This quantity is evaluated only for elements that share a common boundary with the surface. For all other elements this quantity is zero.

Velocity Distribution

The velocities in element e are calculated as in Appendix A, with

$$u = \sum_{j=1}^{9} \frac{1}{a}\frac{\partial N_j}{\partial \xi}(\xi,\eta)\phi_j \tag{A-13}$$

$$v = \sum_{j=1}^{9} \frac{1}{b}\frac{\partial N_j}{\partial \eta}(\xi,\eta)\phi_j \tag{A-14}$$

$$A_{ij} = \frac{1}{90}$$

28/AR +28AR	4/AR -7AR	-1/AR -AR	-7/AR +4AR	-32/AR +14AR	2/AR +8AR	8/AR +2AR	14/AR -32AR	-16/AR -16AR
	28/AR +28AR	-7/AR +4AR	-1/AR -AR	-32/AR +14AR	14/AR -32AR	8/AR +2AR	2/AR +8AR	-16/AR -16AR
		28/AR +28AR	4/AR -7AR	8/AR +2AR	14/AR -32AR	-32/AR +14AR	2/AR +8AR	-16/AR -16AR
			28/AR +28AR	8/AR +2AR	2/AR +8AR	-32/AR +14AR	14/AR -32AR	-16/AR -16AR
				64/AR +112AR	-16/AR -16AR	-16/AR +16AR	-16/AR -16AR	32/AR -128AR
					112/AR +64AR	-16/AR -16AR	16/AR -16AR	-128/AR +32AR
	(SYM)					64/AR +112AR	-16/AR -16AR	32/AR -128AR
							112/AR +64AR	-128/AR +32AR
								256/AR +256AR

$$AR = a/b$$

Figure 32. Elemental Stiffness Matrix for the Quadratic, Lagrange, Element

The x-direction velocity on the top airfoil surface, $\eta=-1$, becomes

$$u_U = \frac{1}{a}\left[\left(\xi-\tfrac{1}{2}\right)\phi_1 + \left(\xi+\tfrac{1}{2}\right)\phi_2 - 2\xi\phi_5\right] \qquad \text{(B-11)}$$

Likewise on the lower surface, $\eta=+1$, u becomes

$$u_L = \frac{1}{a}\left[\left(\xi+\tfrac{1}{2}\right)\phi_3 + \left(\xi-\tfrac{1}{2}\right)\phi_4 - 2\xi\phi_7\right] \qquad \text{(B-12)}$$

<u>Pressure Distribution</u>

For steady small disturbance theory the coefficient of pressure is given by (Ref 13)

$$C_p = -2u \qquad \text{(B-13)}$$

From thin-airfoil theory, the pressure coefficient is evaluated along $y=0^{\pm}$. Thus for element e which borders the airfoil surface the elemental pressure coefficient becomes

$$C_p^e(x, y=0^{\pm}) = \sum_{j=1}^{9} -\frac{2}{a}\frac{\partial N_j}{\partial \xi}(\xi, \eta=\pm 1)\,\phi_j^e \qquad \text{(B-14)}$$

For an upper surface element, $\eta=-1$, C_p becomes

$$C_{p_U}^e = -\frac{2}{a}\left[\left(\xi+\tfrac{1}{2}\right)\phi_3 + \left(\xi-\tfrac{1}{2}\right)\phi_4 - 2\xi\phi_7\right] \qquad \text{(B-15)}$$

For a lower surface element, $\eta=+1$, C_p becomes

$$C_{p_L}^e = -\frac{2}{a}\left[\left(\xi-\tfrac{1}{2}\right)\phi_1 + \left(\xi+\tfrac{1}{2}\right)\phi_2 - 2\xi\phi_5\right] \qquad \text{(B-16)}$$

Within the element e the pressure varies linearly. Since this

element is a C^0 element, there is a jump in pressure from element to element.

Boundary Influence

Elements along the airfoil surface will produce non-zero forcing terms f_i . The forcing terms are determined as in Appendix A, and expressed in A-7 as

$$f_i^e = \int_{\partial\Omega} \frac{df}{dx} N_i \Big|_{y=0^{\pm}} dx \tag{B-17}$$

For a flat plate at angle of attack α , $\frac{df}{dx} = -\alpha$. Converting the integral to the local system gives

$$f_i^e = \int_{\partial\Omega} -\alpha a N_i \Big|_{\eta=\pm 1} d\xi \tag{B-18}$$

For elements along the lower surface the forcing terms are determined from

$$f_i = -\alpha a \int_{-1}^{+1} N_i(\xi, \eta = +1)\, d\xi \tag{B-19}$$

For elements along the upper surface the forcing terms are determined from

$$f_i = -\alpha a \int_{+1}^{-1} N_i(\xi, \eta = -1)\, d\xi \tag{B-20}$$

Appendix C

Finite Element Equations For Flow Over an Airfoil For a Mixed Rectangular Element

Interpolation Functions

The interpolation functions for the mixed rectangular element shown in Fig 33 are given by

$$N_1 = \frac{\xi}{4}(\xi - 1)(1 - \eta) \tag{C-1}$$

$$N_2 = \frac{\xi}{4}(1 + \xi)(1 - \eta) \tag{C-2}$$

$$N_3 = \frac{1}{4}(1 + \xi)(1 + \eta) \tag{C-3}$$

$$N_4 = \frac{1}{4}(1 - \xi)(1 + \eta) \tag{C-4}$$

$$N_5 = \frac{1}{2}(1 - \xi^2)(1 - \eta) \tag{C-5}$$

Coordinates (ξ, η) are the local nodal coordinates.

Elemental Equations

The elemental equations are the same as those derived for the bilinear rectangular element, eq A-5 through A-7

$$A_{ij}\,\phi_j = f_i \tag{A-5}$$

$$A_{ij} = \int_{-1}^{+1}\int_{-1}^{+1}\left(\frac{b}{a}\frac{\partial N_j}{\partial \xi}\frac{\partial N_i}{\partial \xi} + \frac{a}{b}\frac{\partial N_j}{\partial \eta}\frac{\partial N_i}{\partial \eta}\right) d\xi\, d\eta \tag{A-6}$$

$$f_i = a\int_{-1(+1)}^{+1(-1)} \frac{df}{dx}(\xi)\, N_i \Big|_{\eta = \pm 1} d\xi \tag{A-7}$$

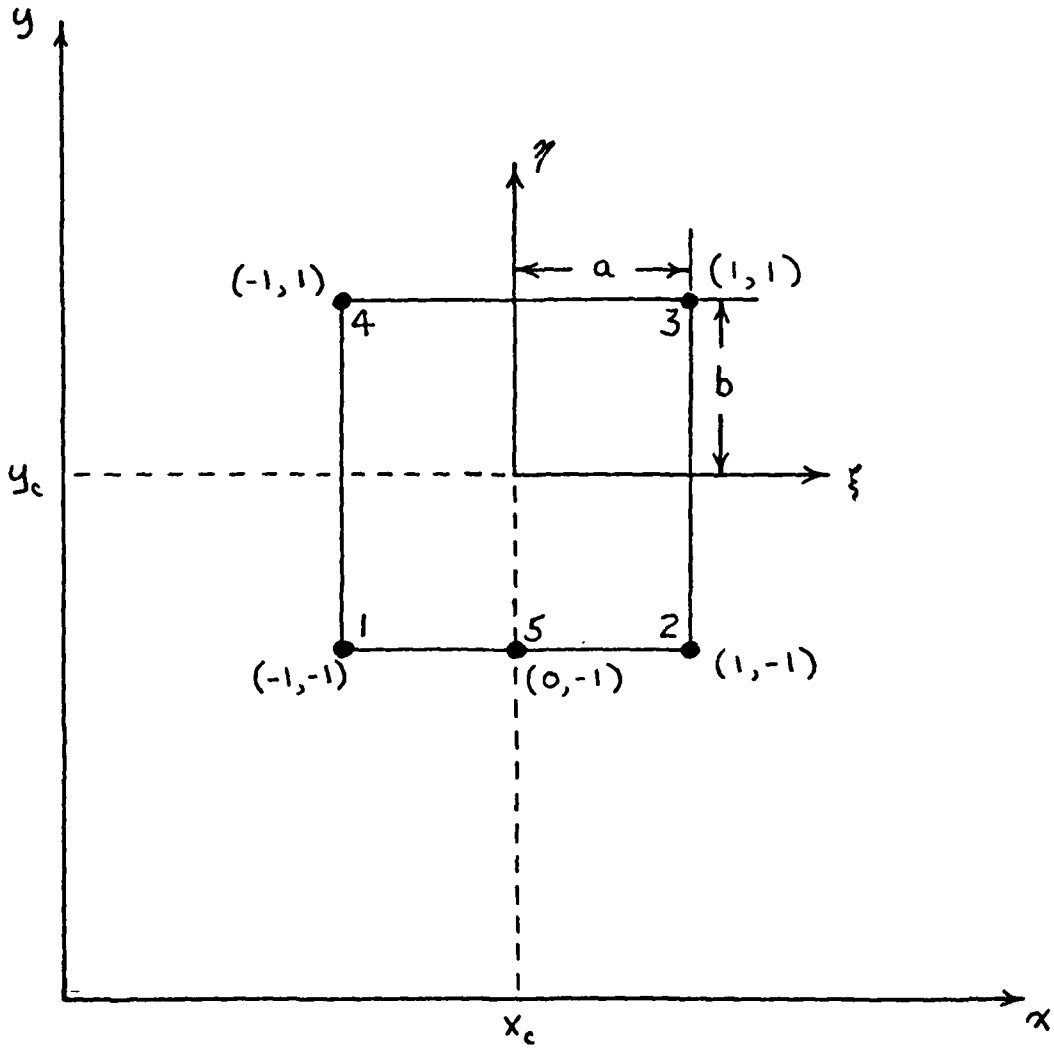

Figure 33. Mixed Rectangular Element

The matrix A_{ij} is only dependent on the size of the element and not directly to any particular airfoil contour. Substituting the interpolation functions, C-1 through C-5, into A-5 results in

$$A_{ij} = \frac{1}{90}\begin{bmatrix} 70/AR + 12AR & 10/AR - 3AR & -15/AR & 15/AR - 15AR & -80/AR + 6AR \\ & 70/AR + 12AR & 15/AR - 15AR & -15/AR & -80/AR + 6AR \\ & & 30/AR + 30AR & -30/AR + 15AR & -30AR \\ & (SYM) & & 30/AR + 30AR & -30AR \\ & & & & 160/AR + 48AR \end{bmatrix} \qquad \text{(C-6)}$$

where $AR = \frac{a}{b}$

The vector f_i is directly dependent on the airfoil surface contour. This quantity is evaluated only for elements that share a common boundary with the surface. For all other elements, this vector is zero.

Velocity Distribution

The velocity in the x-direction on the airfoil is calculated as in Appendix B for the quadratic element. For the upper surface, u becomes

$$u_u = \frac{1}{a}\left[\left(\xi - \tfrac{1}{2}\right)\phi_1 + \left(\xi + \tfrac{1}{2}\right)\phi_2 - 2\xi\phi_3\right] \qquad \text{(C-7)}$$

Pressure Coefficient

The pressure coefficient on the airfoil is calculated as in Appendix B for the quadratic element. For the upper surface, becomes

$$C_p^e = -\frac{2}{a}\left[\left(\xi-\tfrac{1}{2}\right)\phi_1+\left(\xi+\tfrac{1}{2}\right)\phi_2-2\xi\phi_3\right] \qquad \text{(C-8)}$$

Boundary Influence

Those elements e along the airfoil surface will produce non-zero forcing terms f_i . Since the quadratic side of the element is positioned along the airfoil surface, the boundary influence is the same as that derived in Appendix B for the quadratic element.

VITA

John Clifford Gay was born on 18 April 1948 in Biddeford, Maine. He graduated from Biddeford High School in 1966, and attended Wentworth Institute in Boston, Massachusetts. There he received an Associate Degree in Aeronautical Engineering in June 1968. After a short employment with Pratt & Whitney Aircraft, he enlisted in the Air Force in December 1968. Selected for the Airman Education and Commissioning Program, he attended the University of Wyoming where he received a Bachelor of Science Degree in Mechanical Engineering, Aerospace Option in December 1972. After completion of Officer Training School, he received a commission in April 1973. After receiving technical training at Chanute Air Force Base, Illinois, he was assigned as an Aircraft Maintenance Officer, serving tours at Grissom Air Force Base, Indiana; Howard Air Force Base, Canal Zone and Rickenbacker Air Force Base, Ohio. In December 1980, he completed an off-duty education program through Central Michigan University, receiving a Master of Arts in Management and Supervision, Industrial Management. He entered the School of Engineering Air Force Institute of Technology, in June 1980.

Permanent address: 24 Matthews Ave.
Enon, Ohio 45323

SECURITY CLASSIFICATION OF THIS PAGE (When Data Entered)

REPORT DOCUMENTATION PAGE		READ INSTRUCTIONS BEFORE COMPLETING FORM
1. REPORT NUMBER AFIT/GAE/AA/81D-11	2. GOVT ACCESSION NO. AD-A111 123	3. RECIPIENT'S CATALOG NUMBER
4. TITLE (and Subtitle) FINITE ELEMENT ANALYSIS OF SUBSONIC FLOW OVER A LIFTING THIN AIRFOIL		5. TYPE OF REPORT & PERIOD COVERED MS Thesis 6. PERFORMING ORG. REPORT NUMBER
7. AUTHOR(s) John C. Gay Capt USAF		8. CONTRACT OR GRANT NUMBER(s)
9. PERFORMING ORGANIZATION NAME AND ADDRESS Air Force Institute of Technology (AFIT-EN) Wright-Patterson AFB, Ohio 45433		10. PROGRAM ELEMENT, PROJECT, TASK AREA & WORK UNIT NUMBERS
11. CONTROLLING OFFICE NAME AND ADDRESS		12. REPORT DATE December 1981 13. NUMBER OF PAGES 78
14. MONITORING AGENCY NAME & ADDRESS(if different from Controlling Office)		15. SECURITY CLASS. (of this report) Unclassified 15a. DECLASSIFICATION/DOWNGRADING SCHEDULE

16. DISTRIBUTION STATEMENT (of this Report)

Approved for public release; distribution unlimited

17. DISTRIBUTION STATEMENT (of the abstract entered in Block 20, if different from Report)

28 JAN 1982

18. SUPPLEMENTARY NOTES

Approved for public release; IAW AFR 190-17

FREDERIC C. LYNCH, Major, USAF
Director of Public Affairs

19. KEY WORDS (Continue on reverse side if necessary and identify by block number)

Finite Elements
Airfoil Section
Thin-Airfoil Theory
Incompressible Flow

20. ABSTRACT (Continue on reverse side if necessary and identify by block number)

The finite element method was used to solve the flow field problem around a thin, lifting, flat plate, airfoil. The governing equation solved is the Laplace equation, which is valid for inviscid, irrotational, incompressible flow.

The finite element equations were derived through the method of weighted residuals with weighting functions selected by the Galerkin method. For the purposes of analysis, the infinite flow field was

DD FORM 1 JAN 73 1473 EDITION OF 1 NOV 65 IS OBSOLETE

SECURITY CLASSIFICATION OF THIS PAGE (When Data Entered)

replaced by a finite domain. Neumann type boundary conditions were imposed on the airfoil surface. Dirichlet boundary conditions were specified as required by the problem formulation for uniqueness.

Three types of solution methods were used, for various treatments of the jump discontinuity required in the lifting problem. The first method was a superposition technique, which treated the potential along the upper and lower nodes of the branch cut as constant. The circulation was determined by applying the Kutta condition during the combination of the subproblems. The second method was an iterative technique where the circulation was varied until the Kutta condition was satisfied. This method also specified constant potential along the upper and lower branch cut nodes. The third method was also an iterative technique on circulation; however, only the ratio of potentials across the branch cut nodes were kept constant.

Three types of elements were investigated to approximate the solution for the velocity potential function. The first was a bilinear rectangular element. The second was a mixed element with three linear sides and one quadratic side used only on the airfoil surface. All other elements used with it were bilinear. The third element used was a biquadratic, Lagrange, element. The convergence characteristics of each element were studied as a function of the discretization. The pressure distributions are compared with those of classical thin-airfoil theory.

ATE

LMED

-8